Localization and functional role of Tau_{pT217} in Alzheimer's disease

Binita Rajbanshi

Charlottesville,
VA

MSc., University of Bonn, 2017

MS, University of Virginia, 2021

A Dissertation presented to the Graduate Faculty of the
University of Virginia in Candidacy for the
Degree of Doctor of Philosophy

Department of Pharmacology
University of Virginia
November, 2022

Table of Contents

Acknowledgement

I would like to thank my advisor, Professor Dr. Geroge S. Bloom, who has helped me through many years of research assistantship and provided me helpful advice throughout my PhD journey. My work was supported by the Owen's Family Foundation, the Cure Alzheimer's Fund, the Rick Sharp Alzheimer's Foundation, NIH grant RF1 AG051085 to Geroge S. Bloom, and Webb and Tate Wilson. I owe my sincere gratitude to all the patients who donated their brain for my research, without their donation this research would not have taken this shape. I would like to thank Dr. James W. Mandell for supplying human brain samples; Dr. Swapnil Sonkusare for help with dSTORM microscopy; Dr. Ammasi Periasamy, Director of the University of Virginia's W.M. Keck Center for Cellular Imaging, for assistance with FRAP microscopy; NIH equipment grant OD025156 for funding purchase of the Keck Center's Zeiss 980 confocal microscopy system; the late Drs. Lester (Skip) Binder and Peter Davies for respectively providing Tau5 hybridoma cells and PHF1 antibody; Dr. Maria Beatriz Lopes for assisting with pathological staging of human brain sections; Drs. Michael Vitek and Carol Colton for their prior gift of CVN mice; Dr. Anthony J Spano for assistance with preparing plasmids; Dr. Dora Bigler-Wang for handling mice and Dr. Anuj Guruacharya for assistance with statistical analysis. Finally, I would like to thank everyone who has supported me directly or indirectly throughout my PhD journey.

Abstract

Alzheimer's disease (AD) is a progressive neurodegenerative disorder that begins decades before the onset of clinical symptoms of dementia. AD can be distinguished from other neurodegenerative diseases by its pathological hallmarks which are plaques and intracellular neurofibrillary tangles in the brain. The plaques mainly comprise of amyloid-beta (Aβ) peptides while the tangles are primarily composed of a microtubule associated protein called tau. Human central nervous system contains six isoforms of tau. Each isoforms contains 80 potential phosphorylatable sites and ~50 have shown to be phosphorylated. Among those ~50, 3 sites, threonine 181 (T181), threonine 217 (T217) and threonine 231 (T231), were recently found to have high predictive power for early AD symptom onset many years later. However, the functional role of these three phosphorylated sites have been understudied. Among the three phospho-tau variants, tau phosphorylation at T217 (tau_{pT217}) is emerging as a superior predictor of symptom onset as tau positron emission tomography (PET) but little is known about its cellular localization and function in AD pathogenesis. Tau_{pT217} can also be used as a potential therapeutic target if its mechanism of action is properly understood. Thus, understanding the cellular distribution and functional characteristics of tau_{pT217} was the main focus of this dissertation.

To determine the cellular and intracellular deposition, human brain and cultured mouse neurons were analyzed by immunoblotting and immunofluorescence for total tau, tau_{pT217}, tau_{pT181}, tau_{pT231} and $tau_{pS396/pS404}$. Direct stochastic optical reconstruction microscopy (dSTORM) was used to localize tau_{pT217} in cultured neurons. To determine binding affinity of tau phosphorylation at T217 with microtubule and its effect on neurotransmission, tau tagged with enhanced green fluorescent protein was expressed in fibroblasts and in cultured neurons. I used fluorescence recovery after photobleaching (FRAP) to report tau turnover rates on microtubules and calcium imaging to report synaptic function by stimulating or inhibiting AMPA and NMDA receptors.

In this dissertation, I show evidence that in the brain, tau_{pT217} appears in neurons at Braak stages I-II, becomes more prevalent later and co-localizes partially with tau_{pT181} but not with tau_{pT231}. In cultured neurons, tau_{pT217}, is increased by extracellular tau oligomers (xcTauOs), is associated with developing post-synaptic sites, and mediates AMPA and NMDA receptors. Meanwhile, in fibroblasts, FRAP recovery was faster for EGFP-tau_{T217E} than EGFP-tau_{WT}.

The results I have gathered imply that tau_{pT217} increases in the brain as AD progresses and is induced by xcTauOs which may act as seeds in inducing intracellular tau_{pT217} level in AD neurons. Post-synaptic tau_{pT217} suggests a role for T217 phosphorylation in synapse impairment by mediating AMPA and NMDA receptors dependent neurotransmission. My results also imply that reduced microtubule affinity of tau phosphorylated at T217 causes dysregulated fast axonal transport.

This dissertation is an initial step towards understanding early AD therapeutics targeting phospho-tau epitopes. In the future, such strategy could potentially stop or slow AD progression in its early stages itself, rather than later stages.

Keywords: Alzheimer's disease, tau phosphorylation, dendritic spines, neurofibrillary tangles, tau oligomers, neurotransmission

Chapter 1: Tau_{pT217} brings optimism in search for Alzheimer's disease biomarkers and therapeutics

MAIN TEXT

Tau_{pT217} as an early biomarker and early target has become a central focus in the Alzheimer's disease research community recently. Understanding the functional roles of tau_{pT217} provide a ray of hope in the grim outlook of Alzheimer's disease research.

Alzheimer's disease (AD) is a neurodegenerative disorder characterized by progressive memory loss, impaired thinking, and fluctuations in mood and personality [1]. AD can be distinguished from other neurodegenerative diseases by its two main pathological hallmarks which are 1) the development of protein plaques composed of amyloid beta that accumulate outside the cell and 2) the development of neurofibrillary tangles which are composed of tau protein that accumulate in a class of diseases called tauopathies [2]. Officially, AD is one of the leading causes of death in the United States [3]. It is the only disease in the top 10 list with no effective therapy. It's been more than decades since the first AD case was diagnosed back in 1906 by Dr Alois Alzheimer. As of today, AD is still a difficult scientific problem.

The timeline for the onset and progression of sporadic as well as familial AD begins years before neurodegeneration and dementia (Figure 1) [4]. For instance, in the case of sporadic AD, if a patient becomes symptomatic at ~75, synapse loss, plaques and tangles, which are the hallmarks of AD show up in the brain in the late 40's. There is a gap between the appearance of hallmarks in the brain to when the first AD symptom can clinically be diagnosed. By the time a patient becomes symptomatic, there is already massive and irreversible brain damage that can't be treated. The only solution to the futility of AD treatment will therefore be a combination of early diagnosis (perhaps 10 years or longer before symptom onset) and effective early therapy. Early diagnosis and early therapy for AD are the two difficult scientific problems in the AD field.

The current landscape of AD therapeutics, in my opinion, is not very promising. There are three main groups of US-FDA approved drugs for AD (Table 1) : cholinesterase inhibitors, an N-methyl-D-aspartate (NMDA)-receptor antagonist (memantine) and monoclonal antibody. However, the first two types are prescribed for symptomatic patients, for whom they cannot stop or reverse disease progression but can only weakly reduce dementia symptoms for a limited period of time. Another recently approved drug, the monoclonal antibody, Aduhelm (aducanumab), which is still controversial because of its side effects and questionable efficacy. Recent phase 3 trial of Lecanemab have shown highly successful primary and secondary outcomes. Although Lecanemab is based on amyloid, researchers have diversified their research away from the amyloid-based hypothesis that was dominating the field for decades. Researchers are currently either repurposing the government approved drugs for non-AD to AD [5-7] or focusing mainly on tau-based strategies. Most tau-based clinical trials are intended to either reduce or prevent tau aggregation, which occurs later on during AD pathogenesis. So, the outlook for AD looks very grim because of the late therapy after AD symptoms, wrong therapeutic targets, lack

of patients willingness to participate in the trial, and an inadequate understanding of the basic science behind AD pathogenesis.

In accordance with above, the difficult scientific problems in AD can be solved by better understanding of basic science behind the disease. So far, basic science tells us that there are two pathological hallmarks for AD, amyloid plaques and neurofibrillary tangles. However, with the failure of most amyloid targeted therapies, the current focus in the the AD field is on tau protein. Tau is a microtuble (MT) associated protein and was first discovered in the 1970s as the factor that promotes MT assembly [8]. It is normally expressed in neurons, predominantly in axons, where it stabilizes MTs and modulates axonal transport. But when it gets hyperphosphorylated, it is mislocalized [9] and promotes tau aggregation resulting in the formation of neurofibrillary tangles which are hallmarks of AD and other tauopathies [10].

Human central nervous system contains six tau isoforms (Figure 2). Each isoform consists of three major domains: 1) N-terminus which is the projection domain that binds to the membrane-associated structures or motor protein [11], 2) proline rich domain which plays a role in association of tau with actin [12], and 3) C-terminal tail region that includes the assembly domain, three or four tandem imperfect MT binding repeat (MTBR) domains and the flanking regions. All of which supports MT assembly. Each tau isoform can be phosphorylated at different sites. There are 80 theoretically phosphorylatable sites on tau [13] and more than 50 have been shown to be phosphorylated. Among those ~50, 3 sites, threonine 181 (T181), threonine 217 (T217) and threonine 231 (T231), were recently found to have high predictive power for early AD symptom onset many years later [14-16]. However, the functional significance of those sites in AD are not fully understood. Researchers across the globe are comparing plasma phospho-tau epitopes (T181, T217 and T231) with the tau-PET imaging and tau phosphorylation at T217 is emerging as an equal or superior predictor of symptom onset as tau PET. Therefore, tau_{pT217} can be considered as a potential target for early AD therapy, but little is known about its cellular localization and function other than two reports about its histological distribution in AD brain [17, 18].

In accordance with this, the overall goal of my PhD thesis is to determine the localization (Chapter 2) of tau_{pT217} and understand its functional role (Chapter 2, Chapter 3) in AD pathogenesis.

Chapter 2 defines the *in vivo* distribution of tau_{pT217} by surveying brains of human AD patients at various disease stages and in age-matched, cognitively normal controls, in AD model mouse brains, and in cultured mouse neurons. Cultured neurons were also used in chapter 2 to determine if extracellular oligomers of amyloid-β (xcAβOs) or tau (xcTauOs) affect the abundance or localization of tau_{pT217}. Finally, to determine the functional roles of tau phosphorylation at T217 in AD pathogenesis, its effect on affinity for microtubules was examined in chapter 2 and its effect on neurotransmission was determined in chapter 3.

In chapter 2, tau_{pT217} appeared in human brain neurons at Braak stages I-II, and was more prevalent at later disease stages in axons, dendrites, neuronal cell bodies, neuropil threads,

pre-tangles and tangles. In cultured neurons tau_{pT217} was increased by exposure to the extracellular 2N4R tau oligomers (xcTauOs), but not by extracellular amyloid beta-42 oligomers (xcAβOs), and was associated with developing post-synaptic sites. These results raised the possibility that xcTauOs drive T217 phosphorylation of tau *in vivo*, and that tau_{pT217} contributes to synaptic decline which might favor formation of tau-tau interactions at the expense of tau binding to microtubules.

To gain further insight into regulation of tau_{pT217} on neurotransmission, in chapter 3, neuronal synaptic activity was tracked by performing calcium imaging with or without α-amino-3-hydroxy-5-methyl-4-isoxazolepropionic acid (AMPA) receptors or N-methyl-D-aspartate (NMDA) receptors stimulation or inhibition in tau knockout mouse cortical and wild type mouse hippocampal neurons. By doing so, tau phosphorylation at T217 increased both AMPA and NMDA receptors dependent neurotransmission.

Overall, chapter 2 and chapter 3 describes first of its kind studies towards exploring tau_{pT217} functionality as early targets for AD therapy.

FIGURE LEGENDS

FIGURE 1 Onset and progression of sporadic as well as familial AD occur years before neurodegeneration and dementia like symptoms. Adapted from Shaw LM et al., 2007 [4].

FIGURE 2 Six tau isoforms in human central nervous system. Each tau isoforms has 2 or 1 or 0 inserts at the N-terminal half, a proline-rich domain in the middle and 4 or 3 repeat domains towards the C-terminal end.

TABLE 1 Current US-FDA approved drugs for Alzheimer's disease

FIGURES

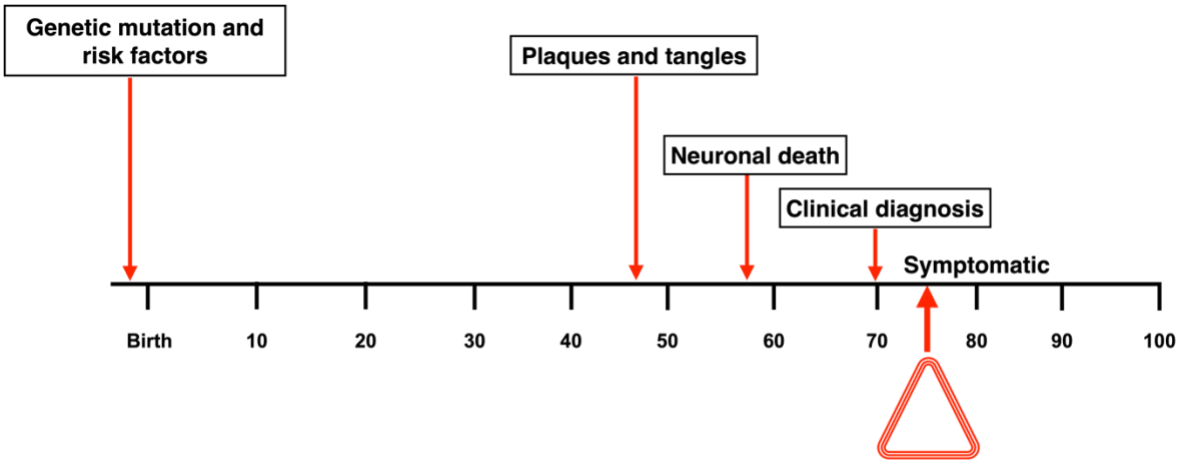

FIGURE 1 Onset and progression of sporadic as well as familial AD occur years before neurodegeneration and dementia like symptoms. Adapted from Shaw LM et al., 2007 [3].

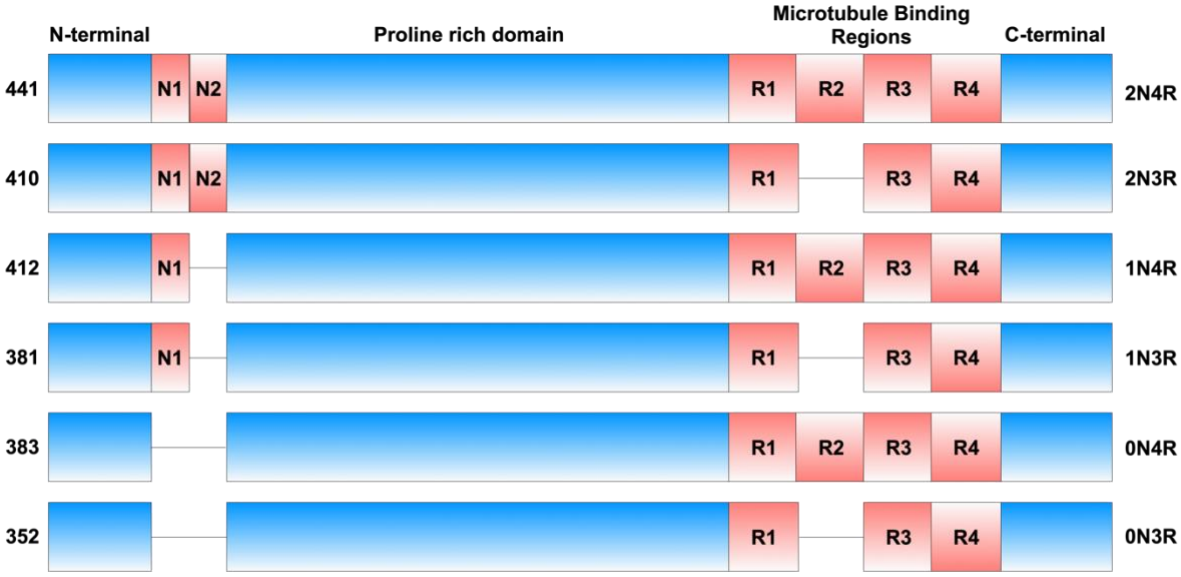

FIGURE 2 Six tau isoforms in human central nervous system. Each tau isoforms has 2 or 1 or 0 inserts at the N-terminal half, a proline-rich domain in the middle and 4 or 3 repeat domains towards the C-terminal end.

Table 1. Current US-FDA approved drugs for Alzheimer's disease

Generic name	Brand name	Year approved	Class	Symptomatic/ disease modifying	MOA
Donepezil	Aricept	1996	Cholinesterase inhibitors	Symptomatic	Prevents ACh breakdown
Rivastigmine	Exelon	2000	Cholinesterase inhibitors	Symptomatic	Prevents ACh and BCh breakdown
Galantamine	Razadyne	2001	Cholinesterase inhibitors	Symptomatic	Prevents ACh breakdown and stimulates nicotinic receptors to release more ACh
Memantine	Namenda	2003	NMDA-Receptor Antagonist	Symptomatic	Blocks toxic effects associated with excess glutamate and regulates glutamate
Memantine + Donepezil	Namzaric	2014	NMDA-Receptor Antagonist + Cholinesterase inhibitors	Symptomatic	Blocks the toxic effects associated with excess glutamate and prevents ACh breakdown
Aducanumab	Aduhelm	2021	Monoclonal antibody	Potential disease modifying	Reduces amyloid plaques present in the brain

Abbreviations
ACh = Acetylcholine
BCh = Butyrylcholine
NMDA = N-methyl D-aspartate
MOA = Mechanism of action

Chapter 2: Localization, induction and cellular effects of tau phosphorylated at threonine 217 in Alzheimer's disease

ABSTRACT

Introduction: Tau phosphorylation at T217 is a promising AD biomarker, but its functional consequences were unknown.
Methods: Human brain and cultured mouse neurons were analyzed by immunoblotting and immunofluorescence for total tau, tau_{pT217}, tau_{pT181}, tau_{pT231} and $tau_{pS396/pS404}$. dSTORM super resolution microscopy was used to localize tau$pT217$ in cultured neurons. EGFP-tau was expressed in fibroblasts as wild type and T217E pseudo-phosphorylated tau, and fluorescence recovery after photobleaching (FRAP) reported tau turnover rates on microtubules.
Results: In brain, tau_{pT217} appears in neurons at Braak stages I-II, becomes more prevalent later and co-localizes partially with other phospho-tau epitopes. In cultured neurons, tau_{pT217}, is increased by extracellular tau oligomers (xcTauOs), and is associated with developing post-synaptic sites. FRAP recovery was fastest for EGFP-tau_{T217E}.
Conclusion: Tau_{pT217} increases in brain as AD progresses and is induced by xcTauOs. Post-synaptic tau_{pT217} suggests a role for T217 phosphorylation in synapse impairment. T217 phosphorylation reduces tau's affinity for microtubules.

Keywords: Alzheimer's disease, tau phosphorylation, dendritic spines, neurofibrillary tangles, tau oligomers, biomarkers

1 | INTRODUCTION

The realization that Alzheimer's disease (AD) comprises a pre-symptomatic phase that might last for more than two decades and that massive, irreversible brain damage has accumulated by the time symptoms are evident has forced a re-evaluation of how to approach the disease clinically. It is now widely accepted that accurate early diagnosis combined with effective interventions that might include drugs and lifestyle adjustments are key to delaying the onset and slowing the progression of AD symptoms, if not preventing symptoms from ever arising. It follows naturally that achieving the tightly linked goals of improved early diagnostics and therapeutics will be aided by a deeper understanding of the molecular mechanisms of AD pathogenesis. While the effort to develop effective therapeutics has not yet yielded any game changing breakthroughs, progress on the diagnostic front has been impressive during the past several years. PET imaging for plaques and tangles is now well established [19-21], and cerebrospinal fluid (CSF) biomarkers have emerged as an alternative approach [22, 23]. PET imaging is sporadically available and costly, though, and obtaining a CSF sample for biomarker analysis requires an invasive procedure in the form of a spinal tap.

Thanks to recent advances in assay sensitivity, it has become possible to substitute blood plasma for CSF to quantify several promising biomarkers for identification of patients at risk of developing AD symptoms years in advance of expected symptom onset. Prime

examples of promising plasma biomarkers are phosphorylated forms of the neuron-specific, axon-enriched, microtubule-associated protein, tau, particularly tau_{pT181}, tau_{pT217} and tau_{pT231} [14-16, 24]. Though several studies have focused on the localization and functional properties of tau_{pT181} [25, 26] and tau_{pT231} [27, 28], little is known about tau_{pT217} other than its promise as an early fluid-based biomarker for AD, and two reports about its histological distribution in AD brain [17, 18].

As a first step toward understanding functional consequences of tau phosphorylation at T217 I sought to define its distribution *in vivo* by surveying brains of human AD patients at various disease stages and in age-matched, cognitively normal controls, in AD model mouse brains, and in cultured mouse neurons. I also used cultured neurons to determine if extracellular oligomers of amyloid-β protein (xcAβOs) or tau (xcTauOs) affect the abundance or localization of tau_{pT217}. Finally, to determine if tau phosphorylation at T217 affects its affinity for microtubules, I expressed EGFP-tagged wild type (WT) and pseudo-phosphorylated tau in fibroblasts, and used fluorescence recovery after photobleaching (FRAP) to measure turnover rates of microtubule-bound tau.

I determined that: 1) tau_{pT217} appears in human brain neurons at Braak stages I-II, and becomes more prevalent at later disease stages in axons, dendrites, neuronal cell bodies, neuropil threads, pre-tangles and tangles that are extensively co-labeled by the AT8 ($tau_{pS202/pT205}$) and PHF1 ($tau_{pS396/pS404}$) antibodies; 2) in cultured neurons, tau_{pT217} is increased by xcTauOs, but not by xcAβOs, and is associated with developing post-synaptic sites; and 3) pseudo-phosphorylation by a T217E amino acid substitution reduces tau's affinity for microtubules. These results raise the possibility that xcTauOs drive T217 phosphorylation of tau *in vivo*, and that tau_{pT217} contributes to synaptic decline and favors formation of tau-tau interactions at the expense of tau binding to microtubules.

2 | METHODS

2.1 | Brain tissue sections

Paraffin-embedded, 5-6 µm thick human cortical brain autopsy sections were obtained from the archives of the Department of Pathology of the University of Virginia, and pertinent clinical information about each donor is shown in Supplementary Table 1. Institutional approval for use of archival autopsy tissue was obtained from the University of Virginia Biorepository and Tissue Research Facility. Classification of disease stages for each donor was performed by ABMS-certified Neuropathologists, James W. Mandell, M.D., Ph.D., and Maria-Beatriz Lopes, M.D., Ph.D., using the "B" (neurofibrillary tangle pathology) part of the ABC staging criteria for AD, in which a score of 0 indicates no detectable tangles, and scores of 1, 2 and 3 respectively correspond to Braak tangle stages I-II, III-IV and V-VI [29].

CVN ($APP_{SwDI}/NOS2^{-/-}$) mice [30] were originally obtained from Drs. Michael Vitek and Carol Colton of Duke University, and were maintained as a breeding colony. 5xFAD ($APP_{SwFlLon}$, $PSEN1_{M146L,\ L286V}$) mouse brain sections were provided by Dr. John Lukens of the University of Virginia Department of Neuroscience. Paraffin-embedded, 5-6 µm

thick sagittal sections of brain tissue were cut following trans-cardiac perfusion of 4% paraformaldehyde in PBS of mice that had been deeply anesthetized intraperitoneally with ketamine/xylazine (280/80 mg/kg). Animals were maintained, bred and euthanized in compliance with all policies of the Animal Care and Use Committee of the University of Virginia.

2.2 | Cultured neurons

As described in the Bloom's lab earlier work, primary mouse cortical neuron cultures were prepared from dissected brain cortices of E16-18 WT C57/Bl6 mice and tau knockout (TKO) mice in the same background strain [31], and were maintained in Neurobasal medium supplemented with B27. For immunofluorescence microscopy, the neurons were grown on 1.5 thickness glass coverslips. All experiments were completed after neurons had been in culture for 10-14 days. Animals were maintained, bred and euthanized in compliance with all policies of the Animal Care and Use Committee of the University of Virginia.

2.3 | CV-1 cells

CV-1 African green monkey kidney fibroblasts were cultured in Dulbecco's modified Eagle's medium supplemented with fetal bovine serum to 10% by volume and 50µg/ml gentamycin.

2.4 | Immunofluorescence microscopy

Human and mouse brain sections were processed identically. First paraffin was removed with a graded series of xylenes. Next, antigen retrieval was performed by immersing brain slides in a beaker of citrate buffer, and then heating in a microwave at high power for 2.5 minutes followed by low power for 8 minutes. Then, the beaker was slowly cooled to room temperature for 20 minutes, after which it was placed in an ice slurry for 20 minutes. Brain sections were then washed with PBS for 5 minutes and incubated with blocking solution (PBS with 5% bovine serum albumin and 0.1% Triton X-100) for 1 hour, followed by sequential incubations for 2 hours each with primary and secondary antibodies. Multiple washes with PBS followed each antibody step, and immediately prior to being sealed with a coverslip using Fluoromount G (ThermoFisher catalog # 00-4958-02) and Hoechst 33342 (ThermoFisher catalog # 62249), sections were washed for 10 minutes with Autofluorescence Inhibitor Reagent (Millipore catalog # 2160).

An analogous procedure was used for immunofluorescence labeling of cultured neurons following fixation and permeabilization for 5 minutes with methanol at -20º C. In this case, though, primary and secondary antibody incubations were for 30-60 minutes each, and the Autofluorescence Inhibitor Reagent step was omitted.

Dephosphorylation of brain sections and neurons was carried out prior to application of primary antibodies by treating with bovine intestinal mucosa alkaline phosphatase (43 µg/ml, Sigma-Aldrich, catalog # P7640) overnight at 4º C.

See Supplementary Table 2 for descriptions of all antibodies used for immunofluorescence and western blotting.

An inverted Nikon Eclipse Ti microscope with planapochromatic 10X and 20X dry, and 40X, 60X and 100X oil immersion objectives, a Yokagawa spinning disk confocal head, 4 diode lasers (405, 488, 561 and 640 nm), and a Hamamatsu Flash 4.0 CMOS camera was used for confocal imaging. Quantification of fluorescence micrographs was performed using the Fiji software derivative of ImageJ, including the Coloc2 plugin for calculating Pearson correlation coefficients.

A dSTORM imaging system (Abbelight; Paris, France) connected to an inverted microscope (DMi8; Leica; Wetzlar, Germany) was used for super resolution microscopy. The microscope was configured with a 63X, NA 1.47 HC planapochromat oil immersion Leica objective and an EM-CCD camera (Sona 4.2B-6; Andor Technology). Fixed and stained cells were embedded in STORM mounting buffer (Abbelight). Fluorophores were excited using 560 nm (200 mW), and 640 nm (500 mW) lasers. Optimal images were obtained through a combination of corrections and background removal using NEO analysis software (Abbelight).

Pearson correlation coefficients were used for analyzing colocalization and student t tests were used for comparing sample sets. For cultured neurons imaged by dSTORM (Figure 4), a minimum of 50 cells per condition from a total of at least 3 biological repeats were used. Graphs were generated using GraphPad Prism 9.0 software. Frequency distribution graphs were generated by first defining each contiguous set of tau_{pT217}-positive pixels and PSD95-positive pixels as a single object. Then, for each tau_{pT217}-positive object I plotted the shortest distance to a PSD95-positive object, and the shortest distance from each PSD95-positive object to a tau_{pT217}-positive object.

2.5 | Fluorescence recovery after photobleaching (FRAP) microscopy

pRK5-EGFP-Tau, a mammalian expression vector encoding an EGFP-human 0N4R tau fluorescent fusion protein was obtained from Addgene (catalog # 46904). This plasmid was developed by the lab of Karen Ashe [9], which generously deposited it with Addgene. 0N4R tau was replaced with 2N4R tau after inserting 2N4R tau between BamHI and SalI restriction sites using a cold fusion cloning kit (System Biosciences, catalog # MC100B-1). A Q5 Site-Directed Mutagenesis Kit (New England BioLabs) was used to convert the WT threonine at position 217 of tau (relative to the largest human CNS tau isoform, 2N4R) to a pseudo-phosphorylated glutamate (T217E). Sequencing of the resulting modified plasmid confirmed the mutation. The new plasmids described here have been deposited in Addgene with plasmid numbers 187023, 187024 and 187025 for EGFP-Tau $_{(WT)}$, EGFP-Tau $_{(T217E)}$ and EGFP-Tau $_{(T217A)}$, respectively.

To measure tau-microtubule interaction in cells, it is necessary to visualize individual microtubules. This can be accomplished using fibroblasts, but not neurons, because neuronal microtubules are too tightly packed to be detected as discrete filaments. WT,

T217E (pseudo-phosphorylated) and T217A (non-phosphorylatable) versions of EGFP-tau, and Venus-Tau-Teal [32] were expressed in CV-1 African green monkey kidney fibroblasts using Lipofectamine 3000 (ThermoFisher). The cells were maintained in phenol red-free Dulbecco's modified Eagle's medium supplemented with fetal bovine serum to 10% by volume and gentamycin to 50 µg/ml.

FRAP microscopy was performed in three sequential steps (see Figure 6A) using a 488 nm excitation laser at the W.M. Keck Center for Cellular Imaging at the University of Virginia: 1) pre-bleach, in which a region of interest (ROI) was selected and imaged at ~1% power to visualize microtubule-bound tau; 2) photobleach the ROI at 50% power; 3) post-bleach time-lapse imaging for 100 seconds at 1 second intervals at 1% power. Images were captured in each interval on a Zeiss 980 laser scanning microscope with a 63X oil immersion planapochromatic objective. Fluorescence intensity in each ROI was plotted as a function of time before and after photobleaching (see Figures 6B-E). The rate of fluorescence recovery of microtubule-associated, photobleached, EGFP-tau is an indicator of the protein's turnover rate on microtubules, and by extension, its affinity for microtubules. Relative to a baseline fluorescence recovery rate, faster recovery indicates more rapid turnover and lower affinity.

To normalize the FRAP data (equation 1), the bleached ROI intensity ($F(t)_{ROI}$) was divided by the whole cell intensity for each time point ($F(t)_{cell}$) after subtracting background fluorescence (F_{bkgd}) at each time point to correct for the loss of fluorescence during the bleach step. The data were then normalized to the pre bleach intensity ($F_{i\text{-}cell}$, $F_{i\text{-}ROI}$) and multiplied by 100 to yield a percentage of initial fluorescence. The resulting normalized data were then averaged for different cells and generated the graphs.

$$\{1\} \quad F(t)_{norm} = 100 \times (F(t)_{ROI} - F_{bkgd})\,(F_{i\text{-}celI} - F_{bkgd}) / (F(t)_{cell} - F_{bkgd})\,(F_{i\text{-}ROI} - F_{bkgd})$$

To calculate the mobile fraction of molecules (*Mf*; equation 2) that recover during the time course of the experiment, I used the data obtained from the normalized recovery curves (equation 1) where F_E, F_0, and F_i are the normalized fluorescence intensities at the end of the experiment, immediately following the bleach, and prior to the bleach, respectively.

$$\{2\} \quad M_f = (F_E - F_0) \quad / (F_i - F_0)$$

I then calculated immobile fraction of molecules (IM_f) by using equation 3.

$$\{3\} \quad IM_f = 1 - M_f$$

Halftime of recovery ($t_{1/2}$), corresponding to 50% of recovered fluorescence intensity ($I_{1/2}$), was then monitored. To compare the halftimes of a molecule under different experimental conditions, ROI size was held constant.

2.6 | Extracellular $A\beta_{1\text{-}42}$ oligomers (xcAβOs)

Lyophilized, synthetic $A\beta_{1\text{-}42}$ (AnaSpec, catalog # AS20276) was dissolved in 1,1,1,3,3,3-hexafluoro 2-propanol (Sigma-Aldrich) to ~1 mM and evaporated for 4 hours at room temperature. The dried powder was resuspended for 5 minutes at room temperature in 40

µl of 20mM sodium hydroxide and sonicated for 10 minutes in a water bath. To prepare xcAβOs, the monomeric peptide was diluted to 400 µl (100 µM final concentration) in Neurobasal medium (GIBCO) and incubated for 48 hours at 4° C with rocking. This was followed by centrifugation at 14,000 g for 15 minutes to remove fibrils and any other large aggregates that may have been present. Cultured neurons were exposed to 2 µM xcAβOs for 16-18 hours before being processed for immunofluorescence or western blotting.

2.7 | Extracellular tau oligomers (xcTauOs)

A bacterial expression plasmid for human 2N4R tau his-tagged at its C-terminus was generously provided by Dr. Nicholas Kanaan of Michigan State University. The protein was expressed in competent BL21 *E. coli* cells induced with 100 mM IPTG and purified from bacterial extracts using TALON beads (Takara Bio, catalog # 635502) according to the vendor's instructions.
I used exactly the same method to prepare xcTauOs as from other groups [33] where they isolated tau oligomers from tau filaments by using sucrose step gradient fractionation, electron microscopy imaging and sandwich ELISA. Purified tau was diluted to 8 µM in a solution of 100 mM NaCl, 5 mM dithiothreitol, 10 mM HEPES (pH 7.6), 0.1 mM EDTA and 300 µM arachidonic acid (AA; Cayman Chemicals, catalog # 90010). The protein was then allowed to aggregate for 18 hours at room temperature in the dark. Resulting xcTauOs were diluted into neuron cultures to yield a final total tau concentration of 250 nM. 24 hours later, cultures were processed for immunofluorescence or western blotting.

2.8 | SDSPAGE and Western blots

Cultured neurons, mouse brains and CV-1 fibroblasts were lysed using N-PER Neuronal Protein Extraction Reagent (ThermoFisher catalog # 87792). Samples were resolved by SDSPAGE using 10% acrylamide/bis-acrylamide gels and transferred to 0.2 µm pore size nitrocellulose (Bio-Rad). Membranes were blocked with Odyssey blocking buffer (LI-COR) and were incubated with primary antibodies and LI-COR secondary IRDye-labeled antibodies diluted into Odyssey blocking buffer. After each antibody step, the blots were washed five times in PBS containing 0.1% Tween 20. The blots were imaged using a BioRad ChemiDoc MP. See Supplementary Table 2 for descriptions of all antibodies used for immunofluorescence and western blotting.

Dephosphorylation of blots was carried out prior to application of primary antibodies by treating with bovine intestinal mucosa alkaline phosphatase (43 – 60 µg/ml, Sigma-Aldrich, catalog # P7640) overnight.

3 | RESULTS

3.1 | The challenge of antibody specificity: presence of the tau_{pT217} epitope in multiple proteins

Throughout the course of this study, the only commercially available antibodies against tau_{pT217} were affinity purified rabbit polyclonal IgG made against a peptide surrounding

pT217 in human 2N4R tau. Products fitting this description are sold by multiple vendors, including but not necessarily limited to ThermoFisher, GenScript, Medimabs, and Abcam, the last of which was the source of the anti-tau$_{pT217}$ that I used. Some vendors, including Abcam, list the immunogen as the LPpTPP peptide that is found in the proline-rich region of all human and mouse tau isoforms, and corresponds to amino acids 215-219 in human 2N4R tau, with the threonine at position 217 being phosphorylated. The other vendors do not specify the immunogen in such detail, but it is possible that they all sell the same product.

Because the peptide used to make Abcam anti-tau$_{pT217}$ was so short, I was concerned that it might be present in other proteins, in which case antibody specificity for tau$_{pT217}$ could be problematic. To determine if the immunogen peptide exists in other mouse or human proteins, I used PhosphoSitePlus to search for proteins with documented threonine phosphorylation within an identical LPpTPP peptide. Numerous perfect hits were detected by the search (see Supplementary Table 3), emphasizing the need to seek conditions in which the anti-tau$_{pT217}$ recognizes only tau phosphorylated at T217.

In light of the potential for anti-tau$_{pT217}$ to recognize multiple proteins I established the following criteria that must be met to justify using the antibody for immunolocalization of tau$_{pT217}$ in cultured neurons and brain tissue. On multiplexed western blots of cultured neuron and brain extracts the antibody must: **1)** label one band or multiple closely spaced bands that co-migrate with bands labeled by the Tau5 mouse monoclonal anti-tau, which recognizes an epitope that is found in all tau isoforms and is not subject to any post-translational modifications [34] ; **2)** the immunoreactive bands must be sensitive to treatment of blots with alkaline phosphatase prior to incubation with anti-tau$_{pT217}$; and **3)** the anti-tau$_{pT217}$ must not label any bands in extracts of brain tissue or cultured neurons derived from tau knockout (TKO) mice. All of those criteria were met by diluting the antigen affinity purified anti-tau$_{pT217}$ 5000-fold to 200 ng/ml (1.43 nM; Supplementary Figure 1). At concentrations of 1 µg/ml (7.14 nM) or higher, though, the Abcam anti-tau$_{pT217}$ also recognized a prominent ~100 kDa protein that is found in WT and TKO mice, and in human brain (not shown) so that band cannot represent any form of tau. Although I have not determined the identity of the ~100 kDa band, based on its size it might represent Map3k14, which is ubiquitously expressed, and like tau$_{pT217}$ contains the LPpTPP sequence. It is important to note that other anti-tau$_{pT217}$ antibodies might be similarly affected by this specificity issue. Examples of such antibodies include the aforementioned rabbit polyclonals sold by vendors that do not divulge the immunogen sequence, and Eli Lilly and Company's IBA493, which is being used for AD biomarker research [17] and is not commercially available.

Another condition I established to inspire confidence that anti-tau$_{pT217}$ specifically and exclusively recognizes tau phosphorylated at T217 for localization is to show by immunofluorescence that staining of brain tissue and primary neuron cultures can be eliminated when the cells or tissue are incubated with alkaline phosphatase prior to the primary antibody step. Supplementary Figure 2 illustrates that when anti-tau$_{pT217}$ is used at 200 ng/ml for immunofluorescence, it preferentially labels neurons in primary mouse cortical neuron cultures that also contain glial cells, as well as in CVN mouse and human

AD brain tissue. Moreover, pretreatment of the cultured cells or brain tissue sections with alkaline phosphatase abolished staining by anti-tau_{pT217}. I thus conclude that using anti-tau_{pT217} at a concentration of 200 ng/ml allows interference-free detection of tau_{pT217} in brain tissue and cultured neurons by both western blotting and immunofluorescence.

Similarly, to the anti-tau_{pT217} antibody, the specificities of mouse anti-tau_{pT181} and mouse anti-tau_{pT231} were tested in primary WT and TKO mouse cortical neurons and brain tissue. At a concentration of 50 ng/ml both anti-tau_{pT181} and anti-tau_{pT231} labeled cultured WT neurons under basal conditions by immunofluorescence (Supplementary Figure 3) but not cultured TKO neurons (Supplementary Figure 4). Likewise, when antibodies to tau_{pT217}, tau_{pT181} and tau_{pT231} were used respectively at 200 ng/ml, 50 ng/ml and 50 ng/ml for immunofluorescence microscopy of CVN and TKO mouse brain, immunoreactivity for each of those antibodies was observed only in the CVN brain (Supplementary Figure 5). When the same antibodies were used for western blotting at that concentration, each labeled a single band that co-migrated with a total tau band labeled by Tau5 in WT neuron extracts, but no immunoreactive bands were observed for extracts of TKO neurons (Supplementary Figure 6). I therefore conclude that the anti-tau_{pT181} and anti-tau_{pT231} antibodies were specific for tau phosphorylated at T181 and T231, respectively, under the conditions in which I used them. Specificity for anti-PHF-1 (pS396/pS404) antibody was also validated in primary WT and TKO mouse cortical neurons at concentration of 45 ng/µl (Supplementary Figure 6).

3.2 | Tau_{pT217} localization in human AD and transgenic AD mouse model brain

To study the in vivo localization of signature AD phospho-tau epitopes, I performed triple immunofluorescence microscopy of human brain sections using antibodies specific for tau_{pT217} and the dendrite-enriched protein, MAP2, plus total tau (detected by the Tau5) antibody), tau_{pT181} (AT180 epitope, but detected by a different antibody), $tau_{pS202/pT205}$ (detected by the AT8 antibody) tau_{pT231}, or $tau_{pS396/pS404}$ (detected by the PHF1 antibody). The human tissue was from 14 individuals ranging in age from 64-95 years old and with Braak stages 0-VI (Supplementary Table 1). The in vivo localization results were intended to serve as a pilot survey of the cellular and intracellular distribution of tau_{pT217}, rather than a comprehensive cataloging of tau_{pT217} localization as functions of disease status and neuroanatomical location in humans.

As shown in Figure 1, tau_{pT217} was barely detectable in human brain cortex at Braak stage 0, when sparse immunoreactivity with antibodies to tau_{pT181} and tau_{pT231} was observed. Appreciable tau_{pT217} immunoreactivity in cortex was first seen at Braak stages I-II, in cytoplasmic puncta, neuropil threads and perinuclear cytoplasm. At those Braak stages some puncta and neuropil threads were labeled by both anti-tau_{pT217} and $antitau_{pT181}$, but staining by the latter was much more extensive. In contrast, tau_{pT217} did not colocalize with tau_{pT231}, which was frequently confined to neuronal nuclei.

At Braak stages III-VI in human brain cortex, illustrated in Figure 2, tau_{pT217} was much more abundant in variably shaped aggregates and perinuclear cytoplasm, and very closely matched the distribution of total tau. Depending on the field of view at those Braak stages,

the tau_{pT217} distribution either resembled or did not match the distributions of tau_{pT181} and tau_{pT231}, the latter of which still was frequently found in neuronal nuclei.

To assess the possible presence of tau_{pT217} in pre-tangles and tangles, human brain sections were labeled with anti-tau_{pT217}, and AT8 or PHF1, the latter two of which are gold standard markers for those structures at advanced Braak stages. I observed extensive overlap between structures labeled by anti-tau_{pT217}, and AT8 (Figure 3) or PHF1 (Supplementary Figure 7) in hippocampus at all Braak stages from I-VI in hippocampus. In cortex, however, PHF1 labeling was mainly in perinuclear puncta, that infrequently co- localized with structures labeled by anti-tau_{pT217} (Supplementary Figure 7). I therefore conclude that at late Braak stages tau_{pT217} is commonly present in pre-tangles and tangles in hippocampus, but less frequently in cortex.

3.3 | Tau_{pT217} is associated with developing post-synaptic sites in cultured neurons

As shown in Supplementary Figures 2 and 3, under basal conditions 10–14-day old, cultured mouse cortical neurons, which reportedly complete synaptogenesis after 15 days in culture [35], express some tau_{pT217} that appears as puncta within MAP2-positive dendrites. The presence of tau_{pT217} in these young WT neurons is consistent with the Tau Phosphorylation Sites table that lists all known, validated phospho-amino acids in tau, including pT217 in the brains of normal and AD humans, and fetal rats. To test the hypothesis that at least some of the puncta correspond to dendritic spines, I double- labeled such neurons with antibodies to tau_{pT217} and the dendritic spine protein, PSD95. When the cells were imaged by a spinning disc laser confocal microscopy with a resolution of ~200 nm in the x-y plane (Figure 4A, B), tau_{pT217} appeared to be extensively co-localized with PSD95, with a Pearson correlation coefficient, of ~0.7 (Figure 4C). The Pearson correlation coefficient measures co-localization on a pixel-by-pixel basis, and importantly the images shown in Figure 4A were not pixel-limited for full optical resolution.

To gain deeper insight into the spatial relation of tau_{pT217} to dendritic spines marked by anti-PSD95, I also examined doubly labeled cells using a dSTORM super-resolution microscope with an x-y resolution of ~15-20 nm (Figure 4B). Under those conditions, the Pearson correlation coefficient was only 0.1 (Figure 4C), although some pixels were positive for both proteins. When combined with the analogous data for confocal microscopy, the dSTORM data indicated that tau_{pT217} is typically located close to dendritic spines, rather than frequently being spatially coincident with them.

Further evidence for association of tau_{pT217} with dendritic spines was obtained by first defining each contiguous set of tau_{pT217}-positive pixels and PSD95-positive pixels as a single object. Then, for each tau_{pT217}-positive object I plotted the shortest distance to a PSD95-positive object, and conversely, the shortest distance from each PSD95-positive object to a tau_{pT217}-positive object. As can be seen in Figure 4D, both types of measurements revealed that most PSD95-positive and tau_{pT217}-positive objects are within 1 µm of each other, with many sharing overlapping pixels and thereby are separated by no more than 15-20 nm. Altogether, these data indicate a very close association of tau_{pT217} with developing dendritic spines.

3.4 | Exposure of cultured neurons to xcTauOs, but not to xcAβOs, increases intraneuronal tau_{pT217}.

xcTauOs and xcAβOs are toxic to neurons and self-propagate in AD brain by prion-like mechanisms [36]. To seek conditions that modulate levels of intracellular tau_{pT217}, I exposed cultured mouse cortical neurons to xcTauOs made from recombinant 2N4R human tau and separately to xcAβOs made from synthetic $A\beta_{1-42}$ (Supplementary Figure 8). The total tau and $A\beta_{1-42}$ concentrations were 250 nM and 2 μM, respectively, and the treatment times were 24 hours for xcTauOs and 16-18 hours for xcAβOs.

As shown in Figure 5, xcTauOs induced an ~56% increase in tau_{pT217} as determined by quantitative immunoblotting, and an ~13% increase as measured by quantitative immunofluorescence microscopy. Statistical signficance was achieved by both methods: $p = 0.0084$ by immunoblotting and $p = 0.0188$ by immunofluorescence. In contrast, tau_{pT217} levels were unaffected by xcAβO exposure as measured by either immunoblotting or immunofluorescence. These results identify xcTauOs, but not xcAβOs, as agents that can increase neuronal levels of tau_{pT217}. In contrast, levels of tau_{pT181} and tau_{pT231} in primary mouse cortical neurons tended to rise after exposure of the cells to xcTauOs, but that increase did not reach statistical significance (Supplementary Figure 9).

3.5 | Phosphorylation at T217 reduces tau's affinity for cytoplasmic microtubules

Tau was originally described as microtubule-associated protein in brain [8], and T217 is found in its proline-rich region (Supplementary Figure 10), which reportedly modulates the structure of the adjacent microtubule-binding repeat domains, and by extension, the affinity of tau for microtubules [37]. Importantly, sub-molecular domains of tau that facilitate tau-tau binding in paired helical filaments [38-41] are embedded within tau's microtubule-binding repeat domains [42]. Conditions that reduce tau's affinity for microtubules might therefore increase tau's propensity to form toxic aggregates.

To test the hypothesis that phosphorylation at T217 affects tau's affinity for microtubules, I expressed EGFP-tagged human 2N4R tau in CV-1 (African green monkey kidney) cells, and performed fluorescence recovery after photobleaching (FRAP) microscopy to study the kinetics of tau turnover on microtubules. CV-1 cells, rather than primary neurons, were used for these experiments, because microtubules in the neurons, but not in the CV-1 cells, are too densely packed to allow microtubule-bound tau to be distinguished from tau that is not associated with microtubules. Two forms of EGFP-tau with respect to the tau sequence were expressed for FRAP: WT and pseudo- phosphorylated T217E (Supplementary Figure 10). As shown in Figure 6A, cells with microtubule-bound EGFP-tau were photographed before and immediately after photobleaching of selective regions of cytoplasm, and at several additional post-bleach times.

Loss of fluorescence in the photobleached areas simply reflected quenching of the EGFP signal, rather than a loss of tau from microtubules. This phenomenon is demonstrated by photobleaching of Venus-Tau-Teal: 2N4R human tau tagged at its N-terminus with Venus fluorescent protein and at its C-terminus with Teal fluorescent protein [32]. As can be seen

in Figure 6B, following complete photobleaching of Venus, microtubules labeled by fluorescent tau can still be clearly seen in the blue-shifted Teal channel that was minimally excited by the photobleaching laser.

As illustrated in Figures 6C-E, the peaks of fluorescence recovery were achieved within ~10 seconds for the T217E forms of EGFP-tau, but the fluorescence intensity of the WT form rose continuously for 100 seconds post-bleaching, and never reached a peak. These results indicate that tau_{pT217} cycles on and off of microtubules much more rapidly than WT tau. I also noticed that microtubules labeled with EGFP-$tau_{(T217E)}$ appeared to be much thinner than those labeled with EGFP-$tau_{(WT)}$. A possible explanation for this observation is that EGFP- $tau_{(T217E)}$ was less densely packed onto microtubules than EGFP-$tau_{(WT)}$.

To verify that the T217E amino acid substitution structurally mimics tau_{pT217}, I used western blotting with anti- tau_{pT217} of CV-1 cells transfected to express EGFP-tau_{WT}, EGFP-tau_{T217E} or EGFP-tau_{T217A}, the latter of which cannot be phosphorylated at position 217 because of the alanine substitution at that site. Prior work has shown that substitution of naturally encoded threonine or serine with glutamate functionally mimics phospho-threonine or phospho-serine, respectively, at multiple amino acid positions in tau [43]. As shown in Supplementary Figure 10, anti- tau_{pT217} recognized EGFP-tau_{WT} and EGFP-tau_{T217E}, but not EGFP-tau_{T217A}. The immunoreactivity with EGFP-tau_{WT} reflects a baseline level of WT tau phosphorylation of T217. More importantly, the immunoreactivity of anti-tau_{pT217} with EGFP-tau_{T217E} and the absence of immunoreactivity with EGFP-tau_{T217A} is consistent with the idea that the T217E amino acid substitution structurally mimics phosphorylation of T217. Altogether, the EGFP-tau expression experiments strongly imply that pseudo-phosphorylation at T217 substantially reduces tau's affinity for microtubules.

4 | DISCUSSION

A flurry of recent studies of potential AD biomarkers has provided evidence that assays for CSF or blood plasma levels of tau_{pT217} can rival or exceed the accuracy of assays for other fluid biomarkers or PET imaging for detecting AD, especially when combined with other diagnostic assays [15, 24, 44]. Indeed, a study that was reported at the Tau 2022 conference but has not been published yet prompted a tentative conclusion that tau_{pT217} levels in CSF define a "clock" that predicts AD progression over a 30 year time span (P-Tau217 Clock). Despite these encouraging advances about the diagnostic value of tau_{pT217} for AD, to the best of my knowledge only one peer-reviewed paper [17] and one published pre-print [18] have addressed the histopathology of tau_{pT217}, and not a single study published until now has investigated what tau_{pT217} does to neurons or what provokes its intracellular accumulation.

To shed more light on the pathobiology of tau_{pT217} I therefore completed a histological survey of its cellular and subcellular distribution in the brains of human AD patients and an AD model mouse strain, and of its cell biological properties in cultured neurons and fibroblasts. Doing so required optimization of an anti- tau_{pT217} antibody that can recognize other proteins with the identical epitope, an issue that likely applies to other antibodies directed against tau_{pT217}. Consistent with prior immunohistological studies of human brain

[17, 18], I found that tau_{pT217} first appears in limbic structure neurons at Braak stages I-II, that its presence in the somatodendritic compartment and neuropil threads increases with disease progression, and that its cellular and subcellular distribution overlaps partially with those of other phospho-tau variants associated with AD and other tauopathies. An immunofluorescence study of aged CVN mice indicates that the tau_{pT217} distribution in this particular AD model mouse strain is similar to what is seen in mid to late-stage human AD, highlighting the potential utility of CVN mice for further studies of tau_{pT217}. Using cultured mouse neurons, I found baseline levels of tau_{pT217} closely associated with nascent dendritic spines, and stimulation of the intracellular tau_{pT217} level by neuronal exposure to xcTauOs, but not to xcAβOs. Finally FRAP analysis of EGFP-tagged tau in fibroblasts implied that phosphorylation of tau at T217 potently decreases tau's affinity for microtubules. Altogether, these new data raise the possibility that phosphorylation at T217 provokes rapid tau turnover on microtubules, concomitant impairment of fast axonal transport [45] and synaptic activity, and stimulation of tau aggregation [46, 47].

Because AD biomarker assays that rely on antibodies to tau_{pT217} are being developed for clinical use, it is essential that such antibodies do not cross-react with other proteins. It is possible that the polyclonal rabbit anti-tau_{pT217} that I used for this study represents the only anti-tau_{pT217} antibody that is currently available from commercial sources, although not all vendors provide sufficient information to be certain. The antibody I used was sold by Abcam and it was produced by immunizing a rabbit with an LPpTPP peptide that is found in at least 18 human and/or mouse proteins other than tau. The possibility that this antibody, as well as the other commercially available rabbit polyclonals and proprietary antibodies to tau_{pT217}, recognize one or more proteins besides tau phosphorylated at T217 is thus a serious concern. Fortunately, I found that diluting the antigen affinity purified antibody 5000-fold to a concentration of 200 ng/ml (1.43 nM) for western blotting of human brain, mouse brain and mouse neuron cultures allowed detection of tau_{pT217} without detecting other bands that were recognized by the antibody when it was used at higher concentrations (Supplementary Figures 1 and 4). I therefore also diluted the antibody to 200 ng/ml for immunofluorescence detection of tau_{pT217}. This concentration-dependent specificity of the antibody presumably reflects protein-specific differences in amino acid sequences that flank the LPpTPP sequence and affect the affinity of the antibody for tau_{pT217} versus other proteins that contain the same peptide. Moreover, antibody dilutions that are sufficient to eliminate spurious immunoreactivity on western blots are direct indicators of the dissociation constants of the antibodies for their respective antigens. When used at such dilutions for other applications, like immunofluorescence and immunohistochemistry, antibody specificities should be as valid as for western blotting because the dissociation constants do not change as long as similar or identical binding and wash buffers are used for all of the various applications. This cautionary tale about the anti- tau_{pT217} antibody that I used should be taken into account for other basic and clinical research studies, as well as clinical applications aimed at detecting tau_{pT217} for all antibodies directed against that tau phosphorylation site.

My immunohistological analysis of tau_{pT217} in human brain yielded results similar to those reported earlier by two other groups [17, 18]. In cortex at Braak stage 0, tau_{pT217} was barely detectable, but occasional immunostaining of axons, neuropil threads and neuronal cell

bodies was evident by Braak stages I-II (Figure 1), and more widespread by Braak stages III-VI (Figure 2). Different immunoreactivity of tau_{pT217} other than tau_{pT181} and tau_{pT231} provides an interesting clue about different functional roles of all three tau variants in AD. This gradual rise in cortical tau_{pT217} immunoreactivity was recapitulated in hippocampus, where frequent labeling of pre-tangles and tangles was also evident at late Braak stages (Figure 3).

In contrast, Moloney and colleagues reported pre-tangles and mature tangles in hippocampus at much earlier Braak stages than I found [18]. Those results were obtained using what may have been a different rabbit polyclonal anti-tau_{pT217} (Thermo-Fisher 44-744) than what I used (Abcam ab192665), however, and at an unspecified nanomolar concentration. The possible use of two different antibodies might therefore explain the discrepancy about how early tau_{pT217}-positive pre-tangles and tangles appear in AD brain, at least in part. Other potential explanations include patient-to-patient variability, post-mortem intervals and lab-specific differences in immunostaining methods.

Frequent hippocampal CA1 tangles containing tau_{pT217} were also reported by Wennström and colleagues, who used a proprietary rabbit anti-tau_{pT217} made by Eli Lilly and Company [17]. Wennström and colleagues also reported that the Lilly antibody robustly labeled granulovacuolar degeneration bodies and multi-vesicular bodies, neither of which I observed. Because further specifications about that antibody are not publicly available, I do not know if it detected tangles and the other structures because it was used at too high a concentration, or if other factors, such as antigen retrieval methods, other aspects of the immunohistochemical protocol might explain the discrepancies with my results.

Interestingly, I found by multi-color immunofluorescence of Braak stages I-VI brain that the distribution of tau_{pT217} was generally similar, but not identical to the distributions of the other phospho-tau epitopes I examined: tau_{pT181}, $tau_{pT202/205}$, tau_{pT231} and $tau_{pS396/pS404}$. Analogous observations were published by Wennström and colleagues[17], but that group did not report the nuclear localization of tau_{pT181} and tau_{pT231} that I observed. A possible explanation for that discrepancy concerns the antibodies that were used. Whereas Wennström and colleagues used AT270 and Abcam EPR2488 to detect tau_{pT181} and tau_{pT231}, respectively, I used Biolegend 846602 to label tau_{pT181} and tau_{pT231}, and Biolegend 828901 for detecting tau_{pT231}. Regardless of what the explanation may be, both the Wennström group and ours agree that each of the phospho-tau epitopes discussed here has a unique cellular and subcellular distribution relative to the others in AD brain. Considering that tau has ~80 potential phosphorylation sites, of which ~50 have been validated (https://bit.ly/2JyZTbS) it should not be surprising that tau phosphorylation does not occur synchronously at its numerous sites. Deciphering how tau phosphorylation at any individual site influences phosphorylatability at other sites, as well as tau function, remain challenging goals.

To gain further insight into functions and regulation of tau_{pT217} I examined its localization and induction in cultured neurons, and used FRAP microscopy to study its association with microtubules in fibroblasts expressing EGFP-tau. Using conventional confocal and

dSTORM super-resolution microscopy, I found a striking correspondence between tau_{pT217} puncta and nascent dendritic spines marked by anti-PSD95 in primary mouse cortical neurons cultured under basal conditions (Figure 4). In addition, exposure of such cultured neurons to xcTauOs caused a substantial increase in intracellular tau_{pT217}, whereas xcAβOs did not affect the level of intraneuronal tau_{pT217} (Figure 5). Finally, I found that tau-EGFP pseudo-phosphorylated at position 217 by a T-to-E amino acid substitution had a dramatically shorter dwell time on fibroblast microtubules than WT tau coupled to EGFP (Figure 6). Altogether, these results raise the possibilities that tau_{pT217} is the pathological form which is involved in synapse dysfunction, that soluble xcTauOs in the brain parenchyma provoke tau_{pT217} accumulation in AD neurons *in vivo*, and that the reduced microtubule affinity of tau phosphorylated at T217 causes dysregulated fast axonal transport, which I described previously as occurring in cultured neurons derived from tau knockout mice [45]. The presence of tau_{pT217} near developing dendritic spines in cultured neurons that are still consolidating synapses [35] suggests a positive role for tau_{pT217} in synapse formation. In contrast, the virtual absence of tau_{pT217} in Braak stage 0 brain and its steady increase at later Braak stages (Figures 1-3 and Supplementary Figure 7) raises the possibility that tau_{pT217} is not involved in synapse maintenance, but that its appearance and buildup during AD pathogenesis is harmful to synapses.

While much further work is required to refine understanding of what causes tau_{pT217} to accumulate in neurons and how it affects neuronal functions, the evidence shown here provides the first indications of how tau_{pT217} might be produced and compromise neuronal health beginning at the earliest stages of AD pathogenesis. At a more clinically relevant level, important questions that arise concern the applicability of the findings presented here to non-Alzheimer's tauopathies, and specifically how these basic science findings might translate to patient care. For example, does tau_{pT217} play pathogenic roles in other mixed tauopathies, such as Parkinson's disease and Huntington's disease, and in pure tauopathies, like Pick's disease and progressive supranuclear palsy? Likewise, while numerous protein kinases can phosphorylate tau at T217 (https://bit.ly/2JyZTbS) would identifying the clinically relevant ones lead to the development of kinase inhibitors or other classes of compounds that interfere with the pathogenesis of AD and other tauopathies for which tau_{pT217} may prove to be important?

FIGURE LEGENDS

FIGURE 1 Tau_{pT217} localization in Braak stages 0-II human brain cortex. Representative fields of view show ~5 μm thick sections labeled with antibodies to tau_{pT217}, MAP2, and total tau (Tau5), tau_{pT181} or tau_{pT231}. All images illustrate single confocal planes.

FIGURE 2 Tau_{pT217} localization in Braak stages III-VI human brain cortex. Representative fields of view show ~5 μm thick sections labeled with antibodies to tau_{pT217}, MAP2, and total tau (Tau5), tau_{pT181} or tau_{pT231}. All images illustrate single confocal planes.

FIGURE 3 Tau_{pT217} localization in Braak stages 0-VI human hippocampus. Representative fields of view show ~5 μm thick sections labeled with antibodies to tau_{pT217}, MAP2 and $tau_{pS202/pT205}$ (AT8 epitope). All images illustrate single confocal planes.

FIGURE 4 Tau_{pT217} is associated with developing dendritic spines marked by PSD95 in cultured mouse cortical neurons. (A) Single plane confocal images taken using a 60X objective. (B) Single plane confocal (100X objective) and dSTORM super-resolution (63X objective) images. (C) Pearson correlation coefficients for quantifying co-localization of tau_{pT217} and PSD95. (D) Frequency distributions of the nearest tau $_{pT217}$-positive structure to each PSD95-positive structure and the nearest PSD95-positive structure to each tau $_{pT217}$-positive structure. At least 50 cells from each of 3 biological replicates with 12 technical replicates apiece for confocal and 3 technical replicates apiece for dSTORM were used to generate the graphs in panels C and D.

FIGURE 5 Tau phosphorylation at T217 is stimulated by extracellular tau oligomers (xcTauOs) made from 2N4R human tau (A), but not by extracellular amyloid-β oligomers (xcAβOs) made from $Aβ_{1-42}$ (B). At least 50 cells from each of 3 biological replicates with 4 technical replicates apiece were used to generate the graphs.

FIGURE 6 T217E pseudo-phosphorylation reduces tau's affinity for microtubules. (A) Fluorescence recovery after photobleaching (FRAP) microscopy summary. FRAP images of CV-1 cells transfected to express Venus-$Tau_{WT\ human\ 2N4R}$-Teal (B), or WT (C) or T217E (D) human 2N4R tau-EGFP. Note in B that photobleaching of Venus did not remove tau from the microtubules, because microtubules were still visible in the Teal channel. (E) Quantification of FRAP. At least 23 cells from at least 3 biological replicates with 3 technical replicates apiece were used to generate the graphs for both EGFP-Tau_{WT} and EGFP-Tau_{T217E}.

SUPPLEMENTARY MATERIAL LEGENDS

Supplementary Figure 1 Validation of anti-tau_{pT217} specificity by western blotting. Anti-tau_{pT217} and total tau (Tau5) western blots were performed against (A) cultured wild type (WT) and tau knockout (TKO) mouse cortical neurons, (B) 24 month old WT and CVN mouse brain homogenates, and (C) elderly, age-matched, cognitively normal and AD human brain homogenates. When used at 200 ng/ml (1.43 nM), as for these experiments, anti-tau_{pT217} labeled a single band with the same electrophoretic mobility as total tau, and

the band was sensitive to alkaline phosphatase treatment prior to the primary antibody step and was undetectable in TKO mouse brain.

Supplementary Figure 2 Validation of anti-tau$_{pT217}$ specificity by immunofluorescence. Braak stage V-VI human brain (A), 24 month old CVN mouse brain (B) and cultured WT mouse cortical neurons were double-labeled with anti-tau$_{pT217}$ at 200 ng/ml (1.43 nM), and to mark the neuronal somatodendritic compartment, with anti-MAP2. Note that anti-tau$_{pT217}$ was sensitive to prior treatment of the tissue sections or cells with alkaline phosphatase.

Supplementary Figure 3 Tau$_{pT217}$ is partly co-localized with tau$_{pT181}$, tau$_{pT231}$ and tau$_{pS396/pS404}$ in WT mouse cortical neurons cultured under basal conditions. Neurons were obtained from E16-E17 embryonic brain and were cultured for 10-14 days. Single plane confocal images are shown.

Supplementary Figure 4 Tau$_{pT217}$, tau$_{pT181}$ and tau$_{pT231}$ are detectable by immunofluorescence microscopy in 14 days old WT, but not TKO mouse cortical neurons. Single plane confocal images are shown.

Supplementary Figure 5 Tau$_{pT217}$, tau$_{pT181}$ and tau$_{pT231}$ are detectable by immunofluorescence microscopy in 18-24 month old CVN, but not in TKO mouse brain. Single plane confocal images are shown.

Supplementary Figure 6 Western blotting validation of mouse anti-tau$_{pT181}$, mouse anti-tau$_{pT231}$ and mouse anti-tau$_{pS396/pS404}$ (PHF1) antibodies in 10-14 day old primary WT and TKO mouse cortical neurons. Tau5 was used as a total tau marker.

Supplementary Figure 7 Tau$_{pT217}$ localization in Braak stages I-VI human brain cortex versus hippocampus. Representative fields of view show ~5 μm thick sections labeled with antibodies to tau$_{pT217}$, MAP2, and tau$_{pS396/pS404}$ (PHF1 epitope). All images illustrate single confocal planes.

Supplementary Figure 8 Analysis of extracellular oligomers of 2N4R human tau and Aβ_{1-42} by western blotting. Tau5 was used to probe the tau blot and 6E10 was used to probe the Aβ_{1-42} blot. *Classification of the indicated immunoreactive bands as dimer and trimer is based on mass spectrometry analysis of similarly sized tau oligomers prepared using arachidonic acid, the same method used in this study, in Patterson, et al. 2011. *J Biol. Chem.* 286: 23063-23076.

Supplementary Figure 9 Tau phosphorylation at T181 and T231 are not stimulated by extracellular tau oligomers (xcTauOs) made from 2N4R human tau. At least 3 biological replicates with 3 technical replicates apiece were used to generate the graphs.

Supplementary Figure 10 EGFP-tau variants used for fluorescence recovery after photobleaching (FRAP) microscopy. The fluorescent fusion proteins were expressed in CV-1 cells as WT, T217E pseudo-phosphorylated and T217A non-phosphorylatable

versions of 2N4R human tau. Note that by western blotting anti- tau_{pT217} labeled EGFP-tau_{WT} and EGFP-tau_{T217E}, but not EGFP-tau_{T217A}, indicating that the T217E amino acid substitution accurately mimics that structure of the tau_{pT217} epitope.

Supplementary Table 1. Clinical characterization of human autopsy brain samples used in the study.

Supplementary Table 2. Primary and secondary antibodies used in the study.

Supplementary Table 3. Human and mouse proteins containing the LPpTPP sequence (from PhosphoSite Plus: https://www.phosphosite.org/homeAction).

FIGURES

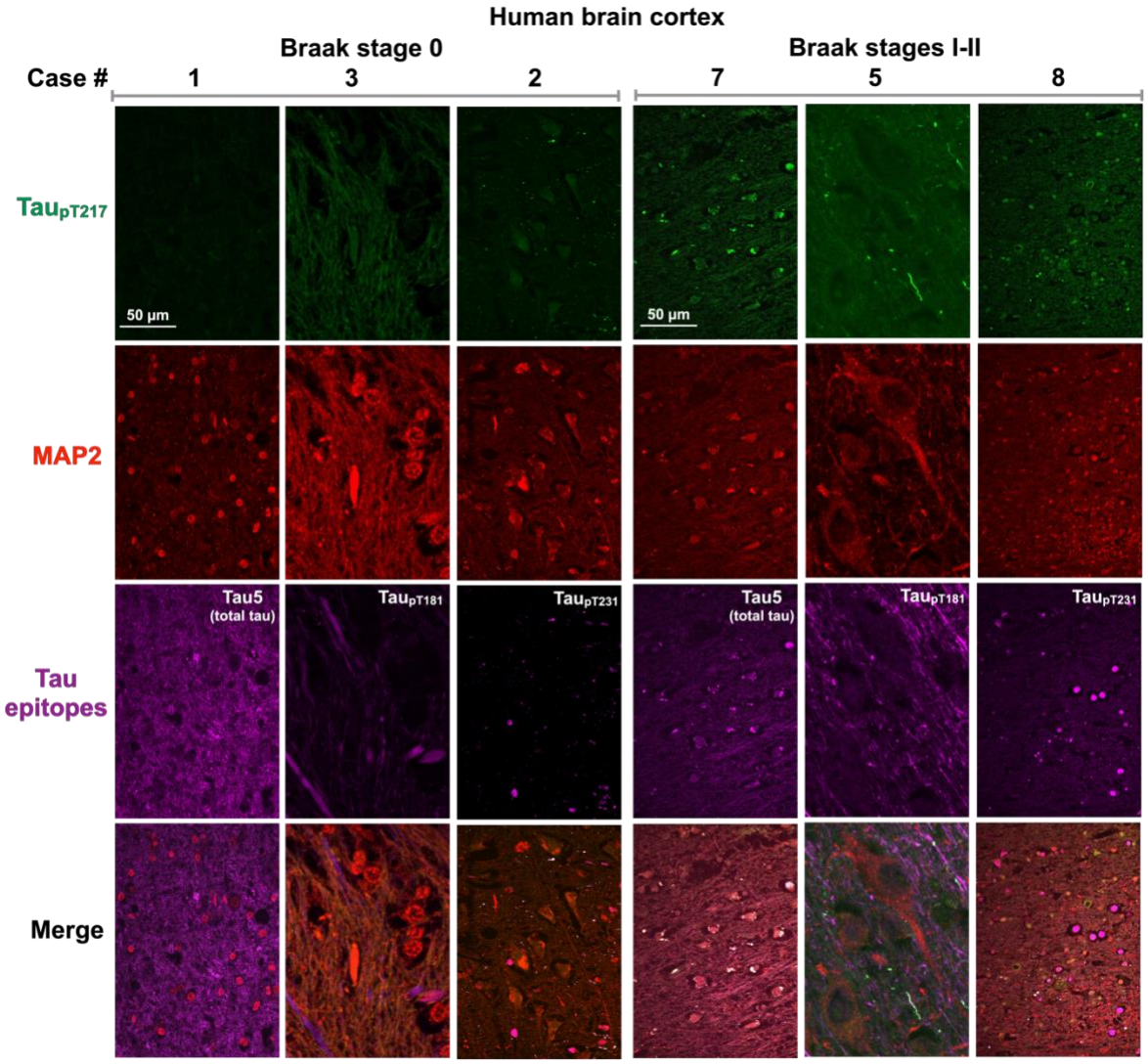

FIGURE 1 Tau_{pT217} localization in Braak stages 0-II human brain cortex. Representative fields of view show ~5 µm thick sections labeled with antibodies to tau_{pT217}, MAP2, and total tau (Tau5), tau_{pT181} or tau_{pT231}. All images illustrate single confocal planes.

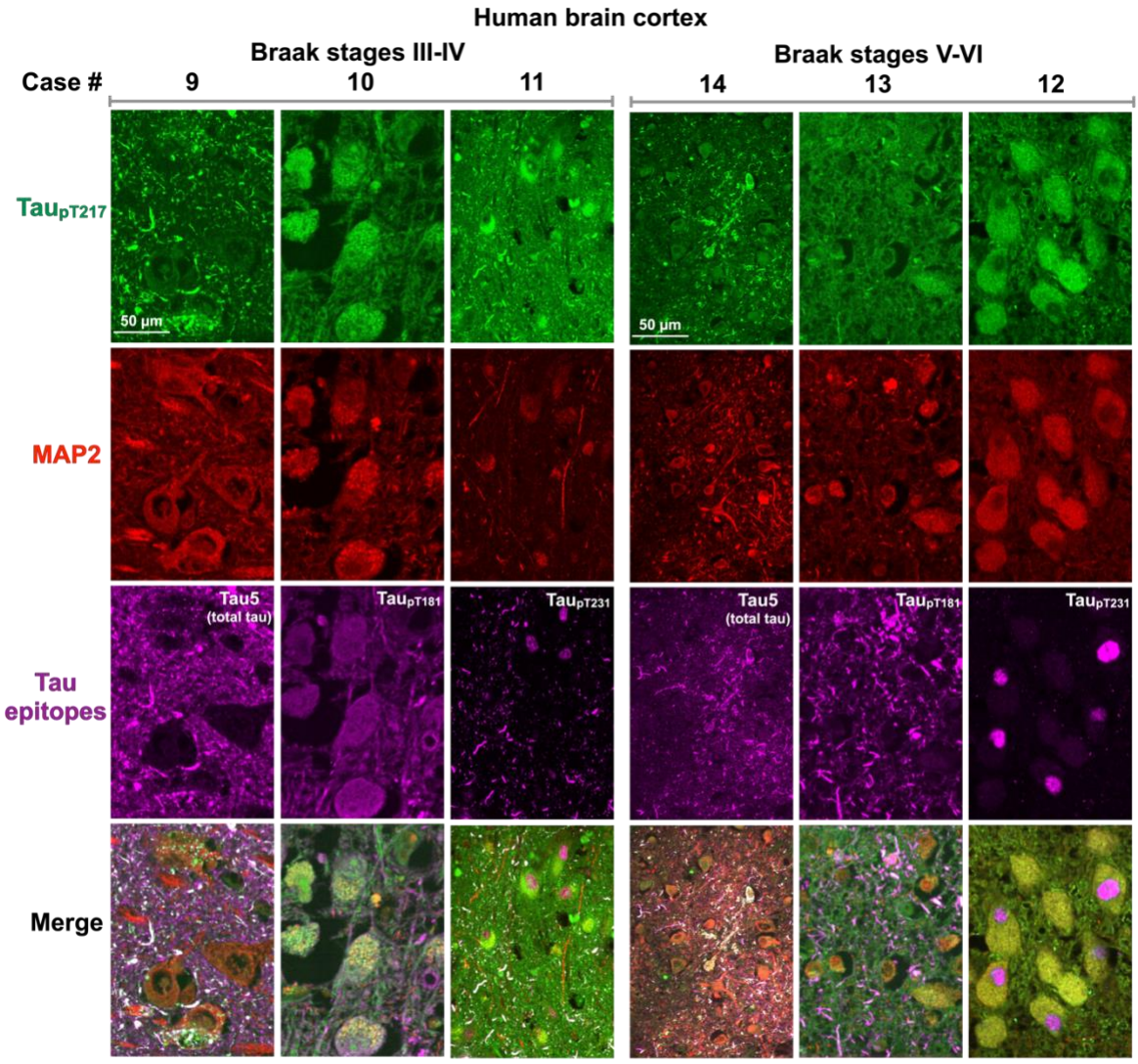

FIGURE 2 Tau_{pT217} localization in Braak stages III-VI human brain cortex. Representative fields of view show ~5 µm thick sections labeled with antibodies to tau_{pT217}, MAP2, and total tau (Tau5), tau_{pT181} or tau_{pT231}. All images illustrate single confocal planes.

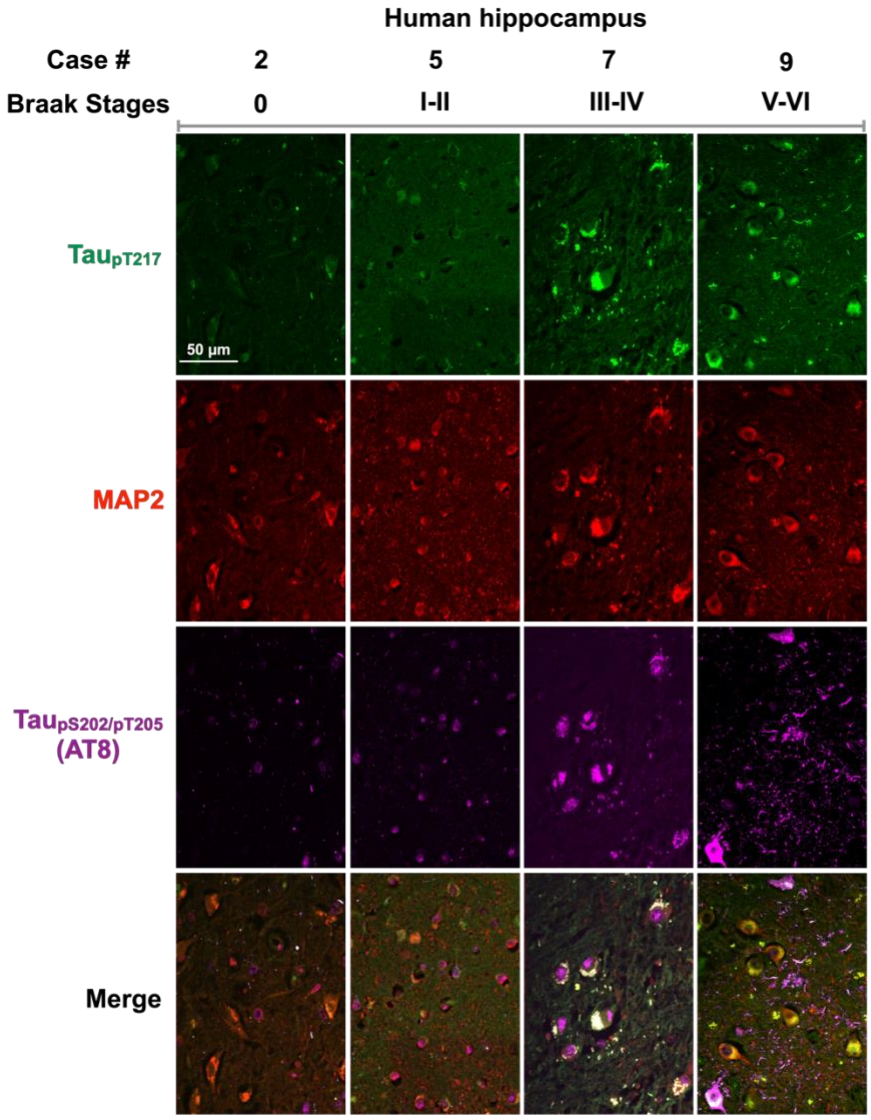

FIGURE 3 Tau_{pT217} localization in Braak stages 0-VI human hippocampus. Representative fields of view show ~5 µm thick sections labeled with antibodies to tau_{pT217}, MAP2 and $tau_{pS202/pT205}$ (AT8 epitope). All images illustrate single confocal planes.

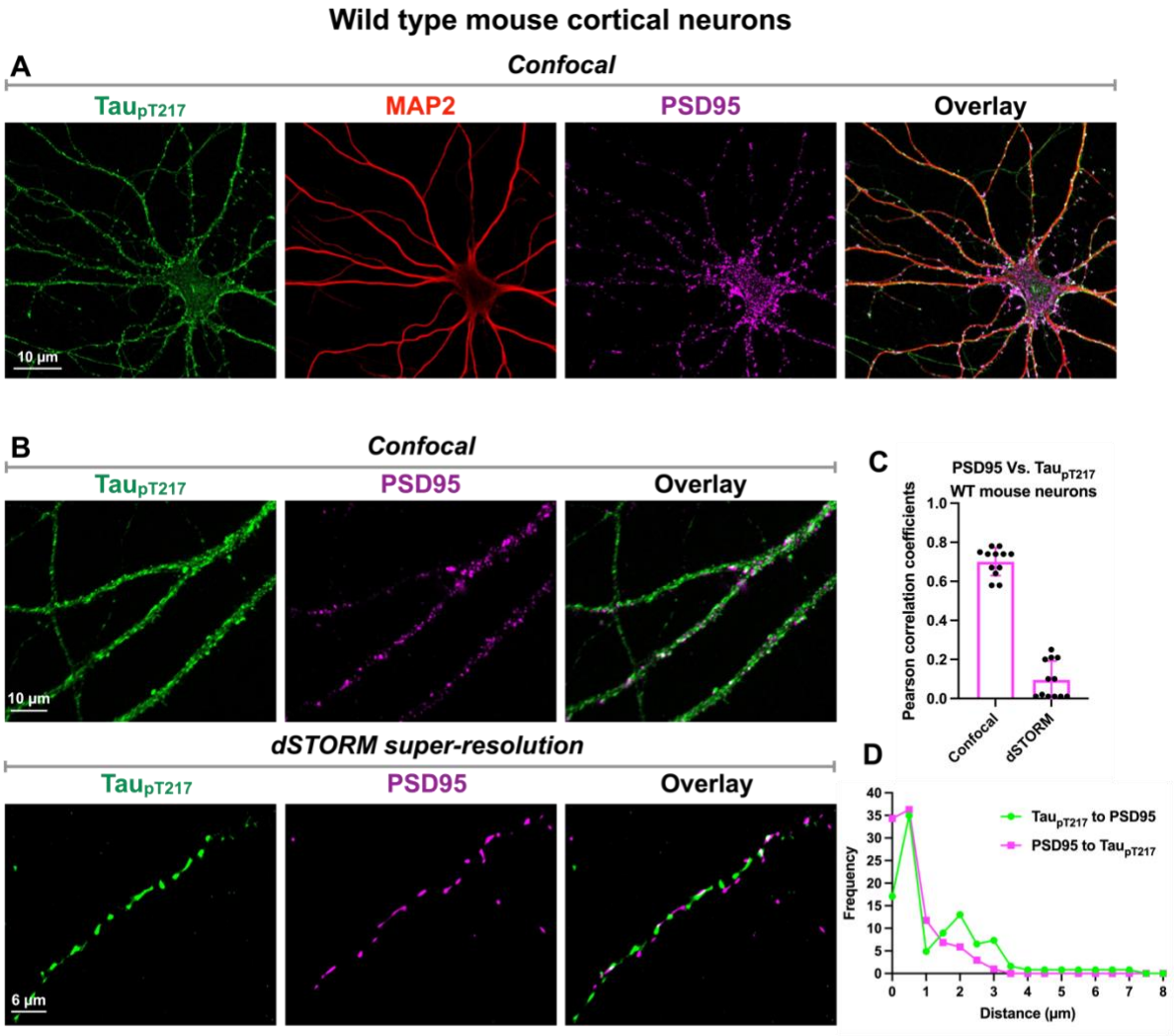

FIGURE 4 Tau_{pT217} is associated with developing dendritic spines marked by PSD95 in cultured mouse cortical neurons. (A) Single plane confocal images taken using a 60X objective. (B) Single plane confocal (100X objective) and dSTORM super-resolution (63X objective) images. (C) Pearson correlation coefficients for quantifying co-localization of tau_{pT217} and PSD95. (D) Frequency distributions of the nearest tau $_{pT217}$-positive structure to each PSD95-positive structure and the nearest PSD95-positive structure to each tau $_{pT217}$-positive structure. At least 50 cells from each of 3 biological replicates with 12 technical replicates apiece for confocal and 3 technical replicates apiece for dSTORM were used to generate the graphs in panels C and D.

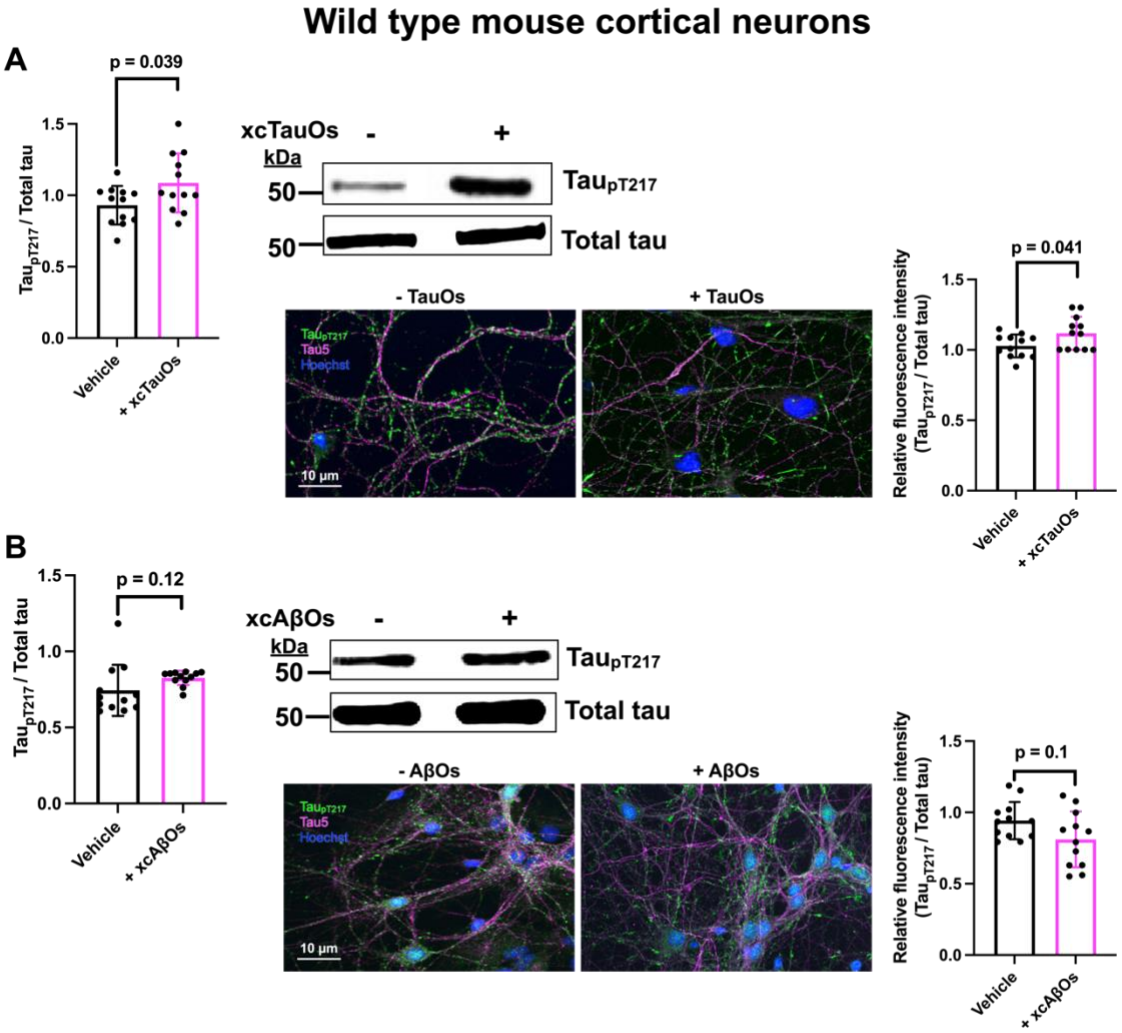

FIGURE 5 Tau phosphorylation at T217 is stimulated by extracellular tau oligomers (xcTauOs) made from 2N4R human tau (A), but not by extracellular amyloid-β protein oligomers (xcAβOs) made from $Aβ_{1-42}$ (B). At least 50 cells from each of 3 biological replicates with 4 technical replicates apiece were used to generate the graphs.

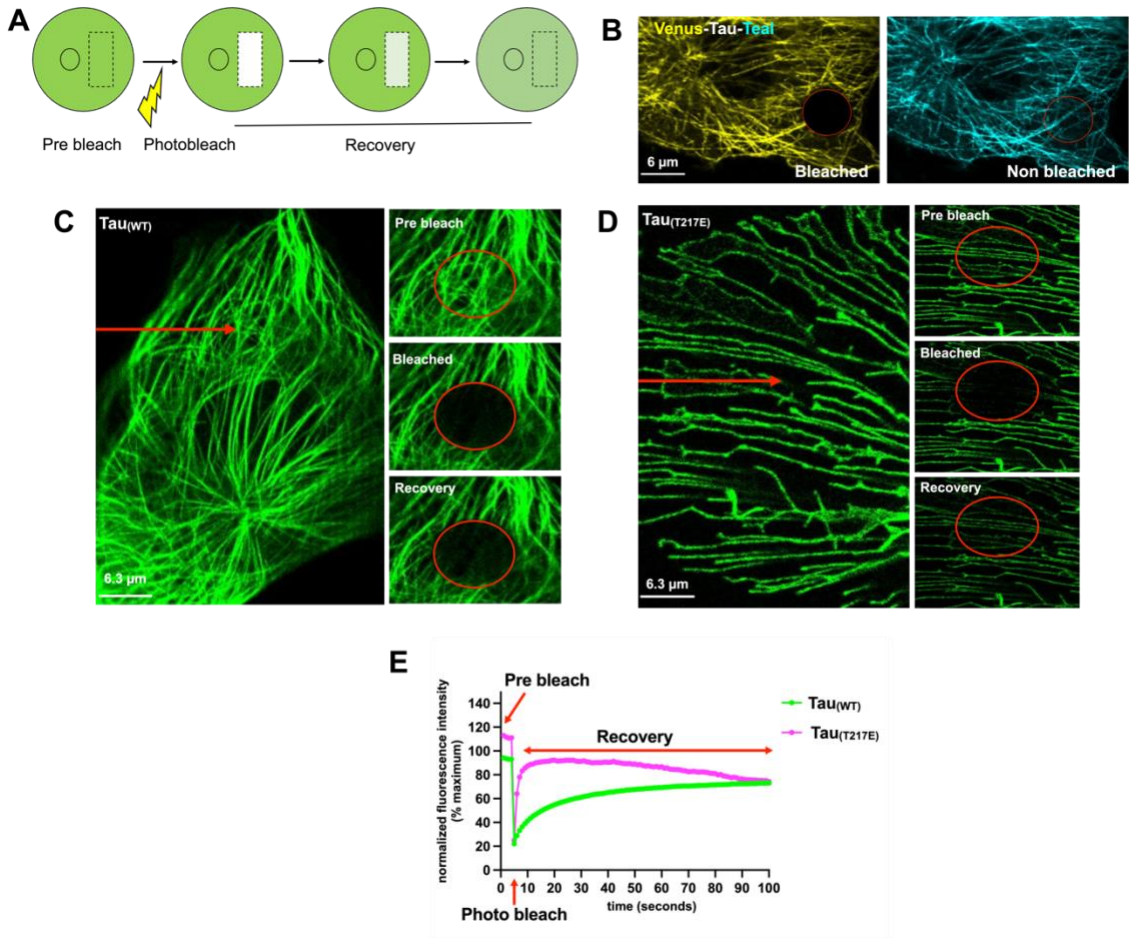

FIGURE 6 T217E pseudo-phosphorylation reduces tau's affinity for microtubules. (A) Fluorescence recovery after photobleaching (FRAP) microscopy summary. FRAP images of CV-1 cells transfected to express Venus-$Tau_{WT\ human\ 2N4R}$-Teal (B), or WT (C) or T217E (D) human 2N4R tau-EGFP. Note in B that photobleaching of Venus did not remove tau from the microtubules, because microtubules were still visible in the Teal channel. (E) Quantification of FRAP. At least 23 cells from at least 3 biological replicates with 3 technical replicates apiece were used to generate the graphs for both EGFP-Tau_{WT} and EGFP-Tau_{T217E}.

SUPPLEMENTARY MATERIALS

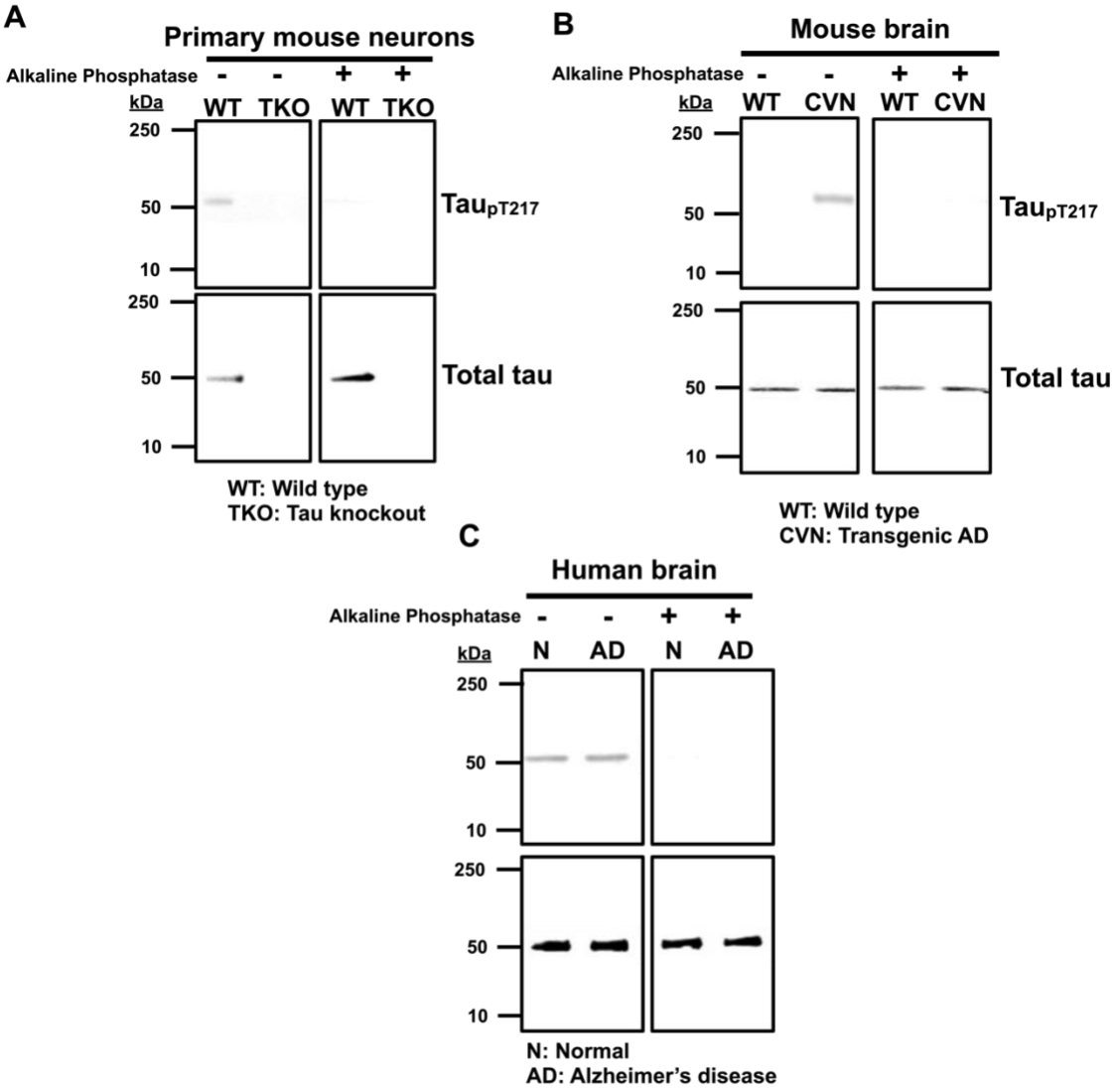

Supplementary Figure 1 Validation of anti-tau$_{pT217}$ specificity by western blotting. Anti-tau$_{pT217}$ and total tau (Tau5) western blots were performed against (A) cultured wild type (WT) and tau knockout (TKO) mouse cortical neurons, (B) 24 month old WT and CVN mouse brain homogenates, and (C) elderly, age-matched, cognitively normal and AD human brain homogenates. When used at 200 ng/ml (1.43 nM), as for these experiments, anti-tau$_{pT217}$ labeled a single band with the same electrophoretic mobility as total tau, and the band was sensitive to alkaline phosphatase treatment prior to the primary antibody step and was undetectable in TKO mouse brain.

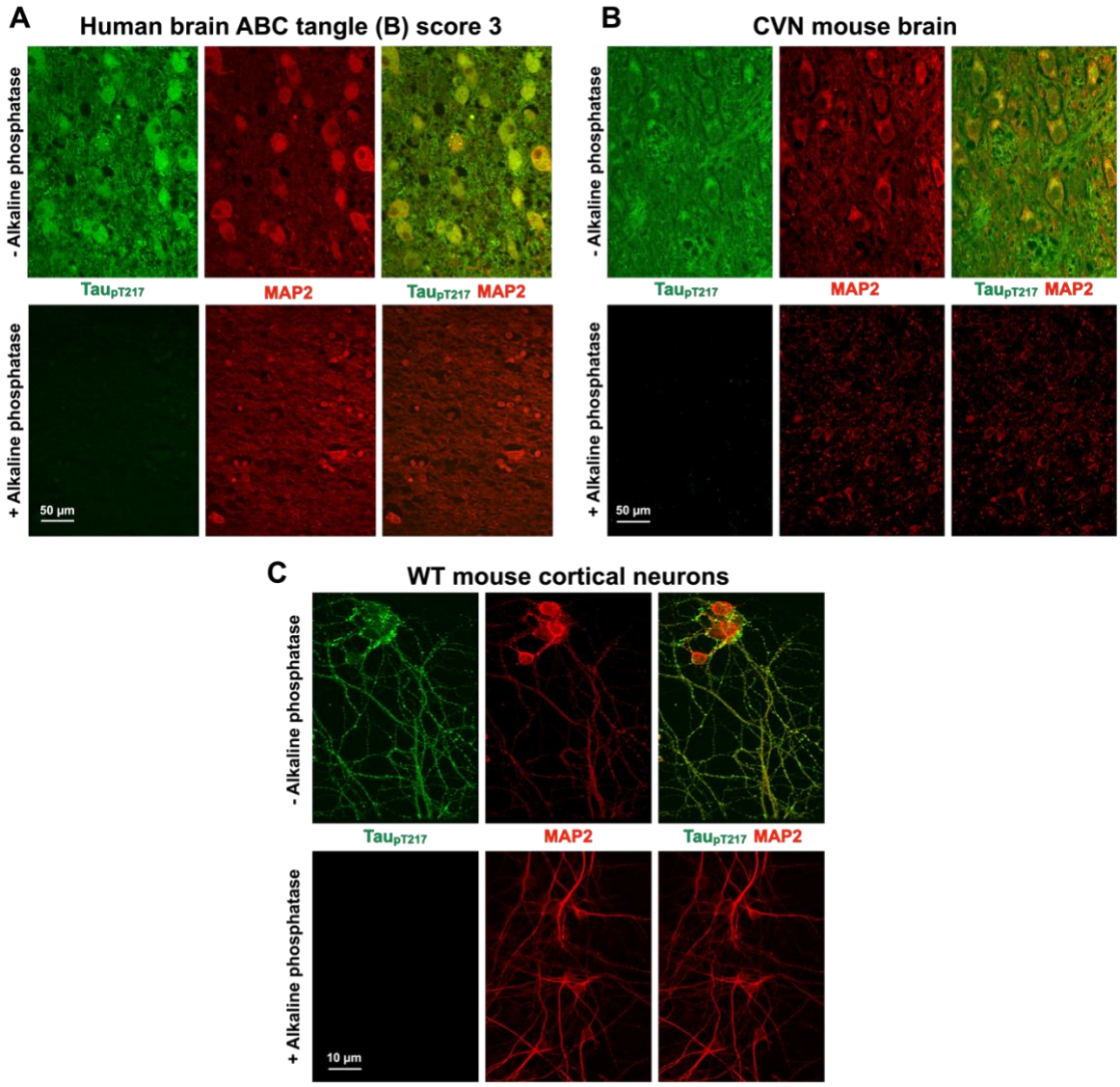

Supplementary Figure 2 Validation of anti-tau$_{pT217}$ specificity by immunofluorescence. Braak stage V-VI human brain (A), 24 month old CVN mouse brain (B) and cultured WT mouse cortical neurons were double-labeled with anti-tau$_{pT217}$ at 200 ng/ml (1.43 nM), and to mark the neuronal somatodendritic compartment, with anti-MAP2. Note that anti-tau$_{pT217}$ was sensitive to prior treatment of the tissue sections or cells with alkaline phosphatase.

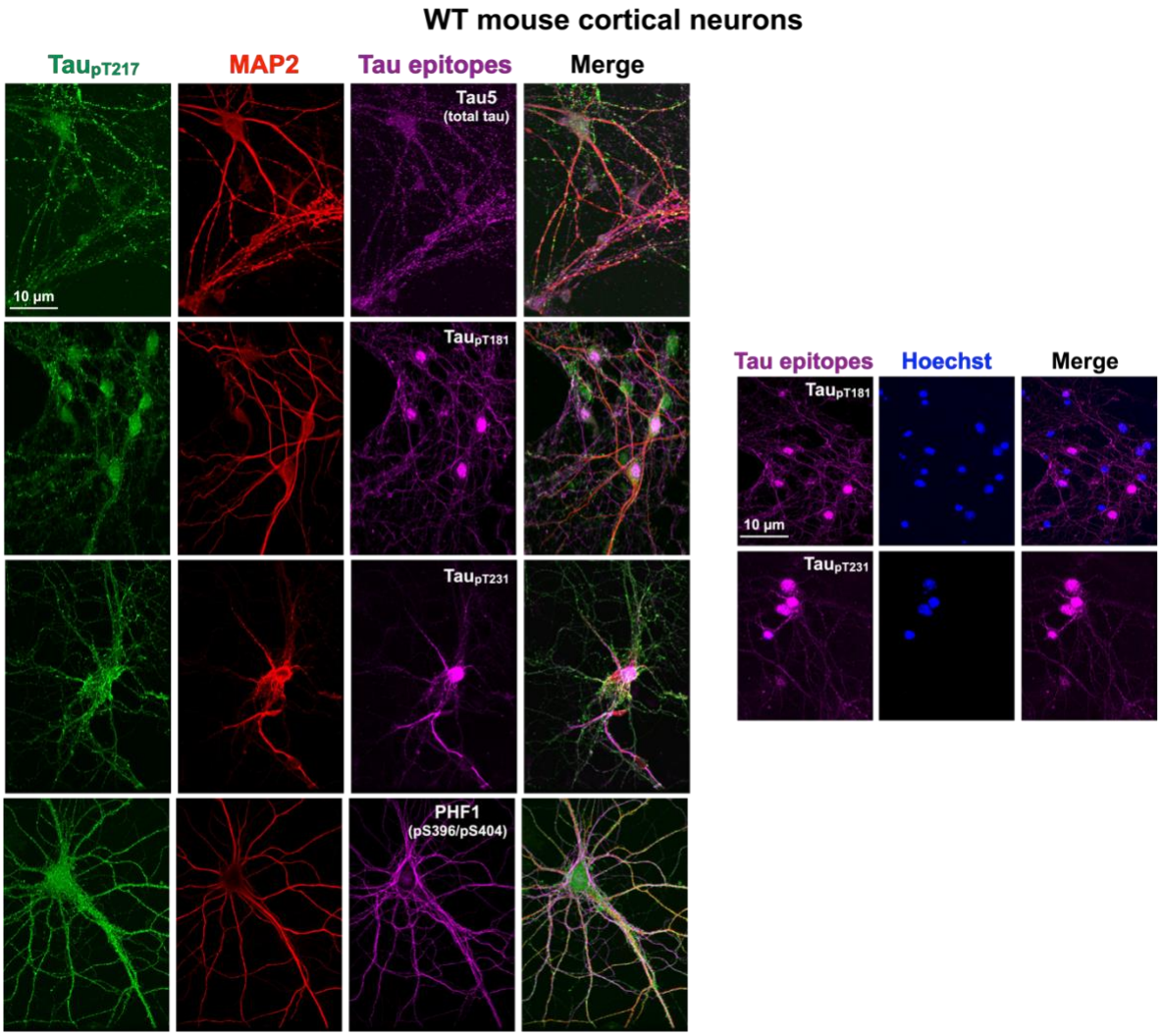

Supplementary Figure 3 Tau_{pT217} is partly co-localized with tau_{pT181}, tau_{pT231} and $tau_{pS396/pS404}$ in WT mouse cortical neurons cultured under basal conditions. Neurons were obtained from E16-E17 embryonic brain and were cultured for 10-14 days. Single plane confocal images are shown.

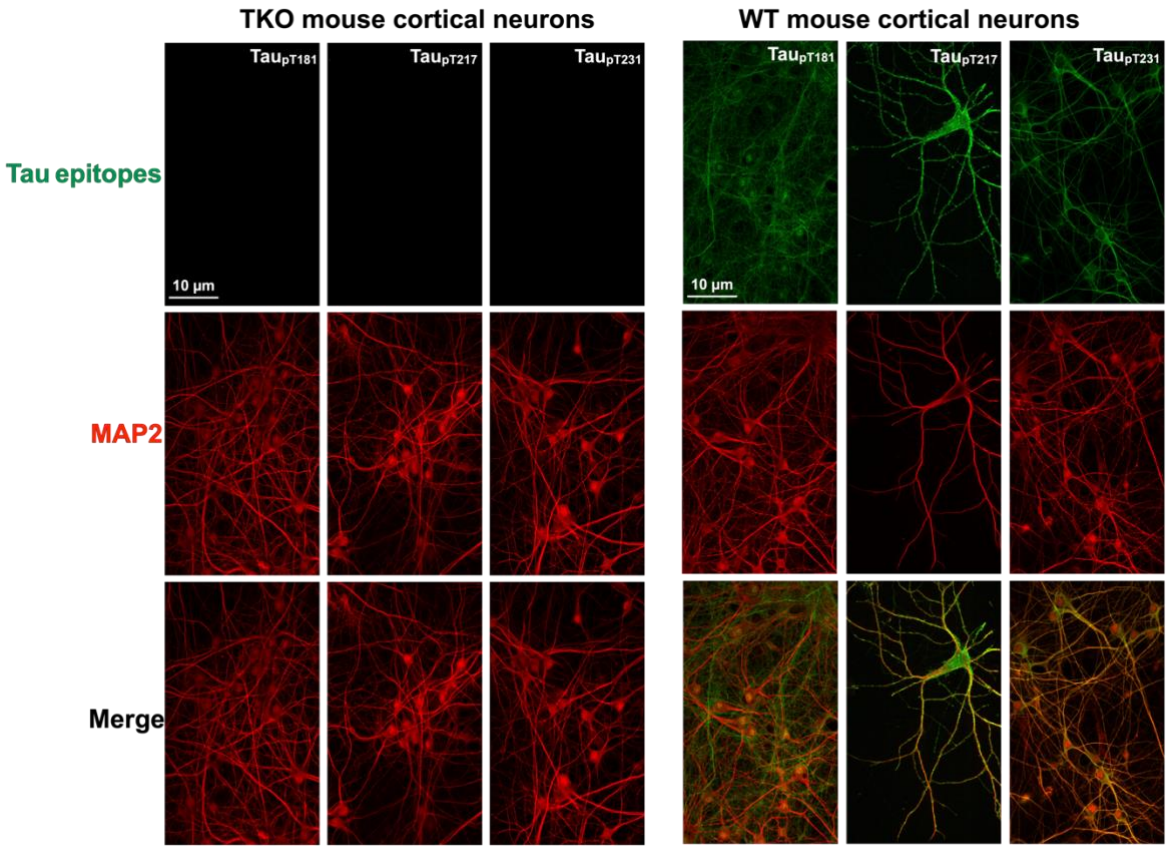

Supplementary Figure 4 Tau_{pT217}, tau_{pT181} and tau_{pT231} are detectable by immunofluorescence microscopy in 14 days old WT, but not TKO mouse cortical neurons. Single plane confocal images are shown.

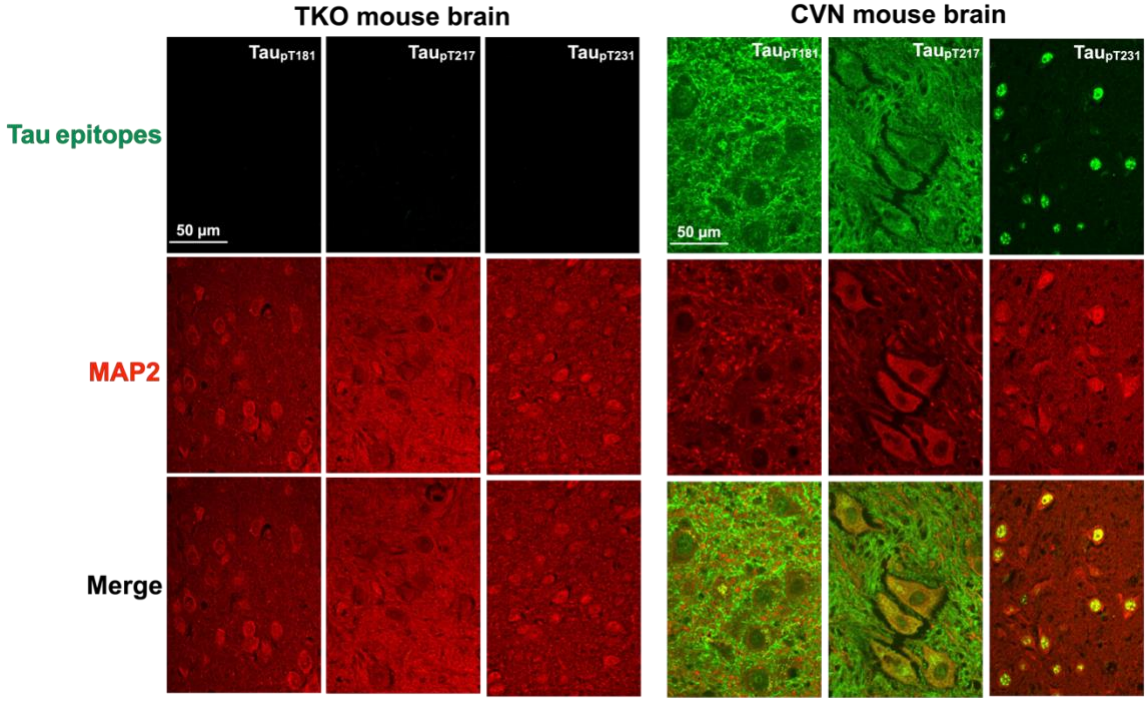

Supplementary Figure 5 Tau_{pT217}, tau_{pT181} and tau_{pT231} are detectable by immunofluorescence microscopy in 18-24 month old CVN, but not in TKO mouse brain. Single plane confocal images are shown.

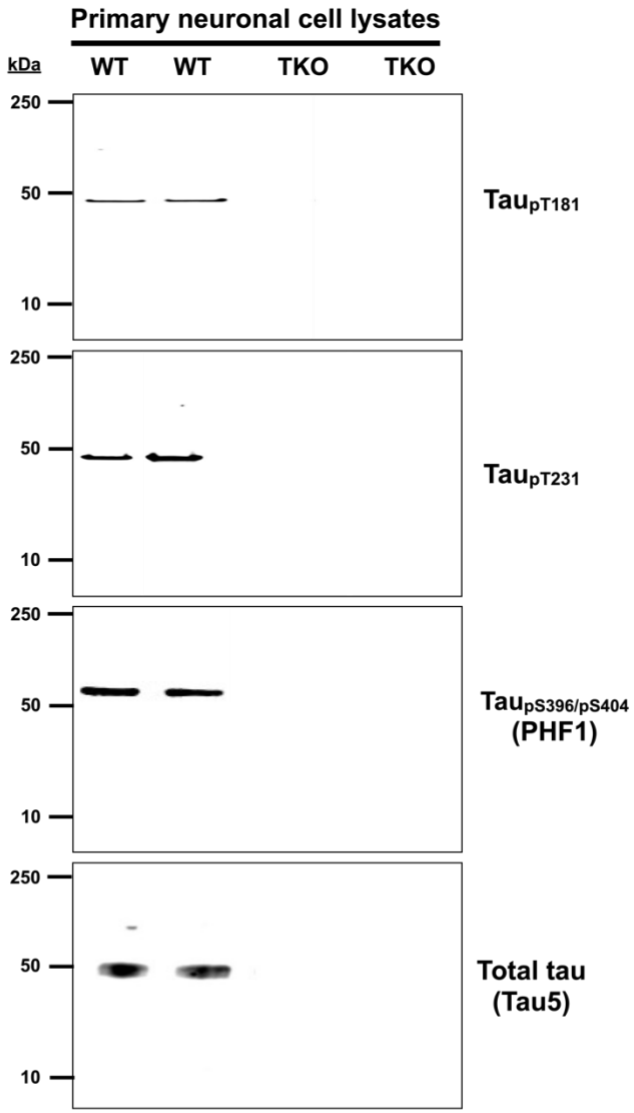

Supplementary Figure 6 Western blotting validation of mouse anti-tau$_{pT181}$, mouse anti-tau$_{pT231}$ and mouse anti-tau$_{pS396/pS404}$ (PHF1) antibodies in 10-14 day old primary WT and TKO mouse cortical neurons. Tau5 was used as a total tau marker.

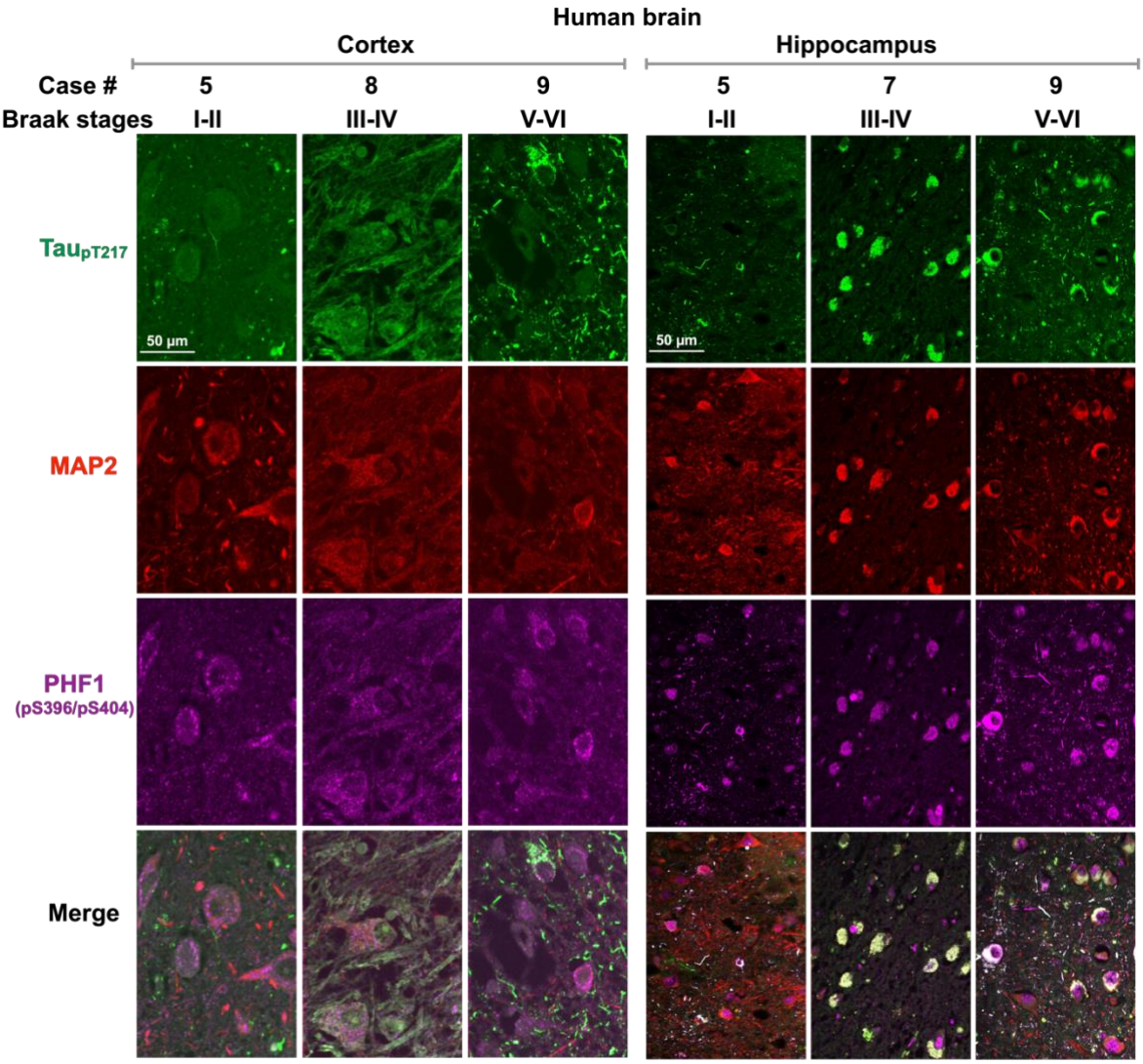

Supplementary Figure 7 Tau_{pT217} localization in Braak stages I-VI human brain cortex versus hippocampus. Representative fields of view show ~5 µm thick sections labeled with antibodies to tau_{pT217}, MAP2, and $tau_{pS396/pS404}$ (PHF1 epitope). All images illustrate single confocal planes.

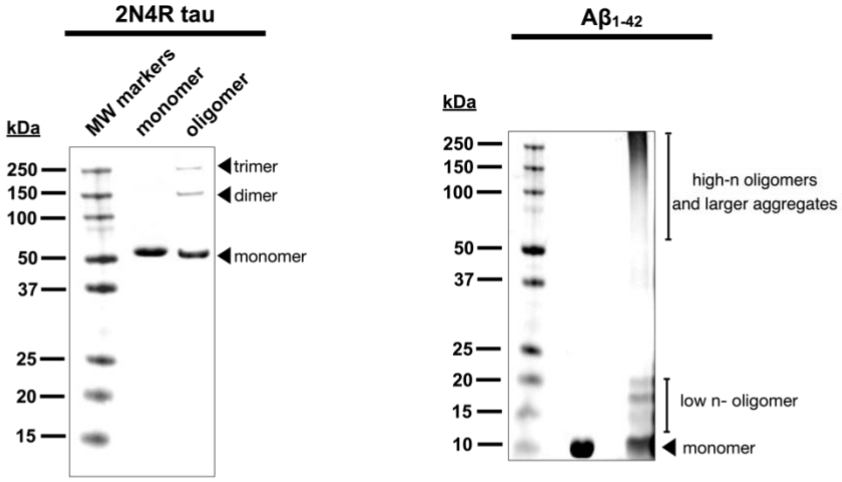

Supplementary Figure 8 Analysis of extracellular oligomers of 2N4R human tau and $A\beta_{1-42}$ by western blotting. Tau5 was used to probe the tau blot and 6E10 was used to probe the $A\beta_{1-42}$ blot.

*Classification of the indicated immunoreactive bands as dimer and trimer is based on mass spectrometry analysis of similarly sized tau oligomers prepared using arachidonic acid, the same method used in this study, in Patterson, et al. 2011. *J Biol. Chem.* 286: 23063-23076.

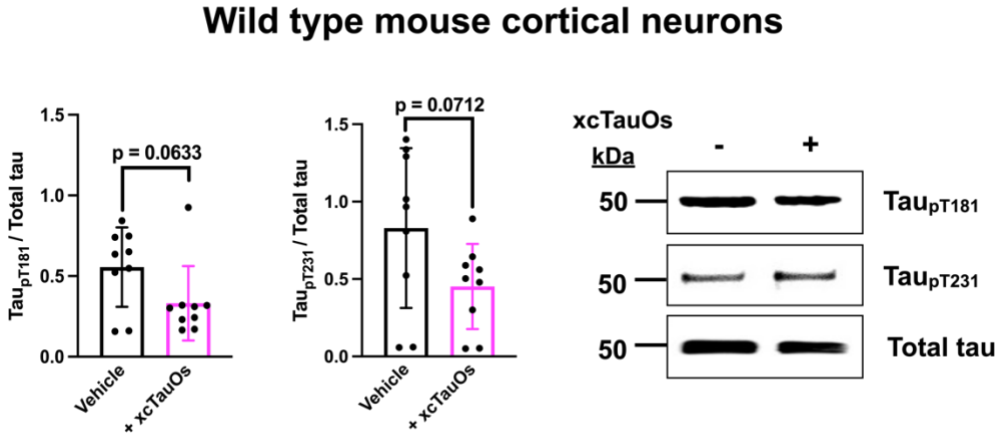

Supplementary Figure 9 Tau phosphorylation at T181 and T231 are not stimulated by extracellular tau oligomers (xcTauOs) made from 2N4R human tau. At least 3 biological replicates with 3 technical replicates apiece were used to generate the graphs.

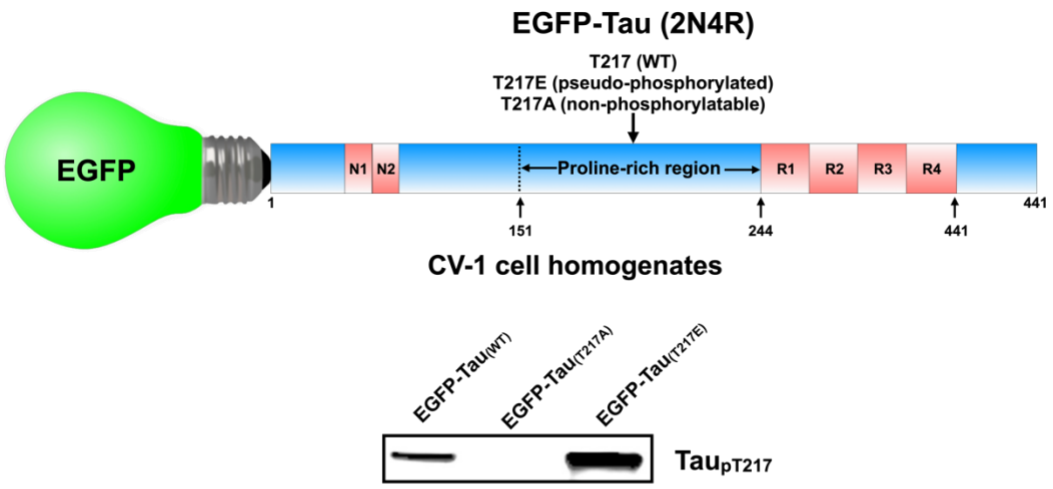

Supplementary Figure 10 EGFP-tau variants used for fluorescence recovery after photobleaching (FRAP) microscopy. The fluorescent fusion proteins were expressed in CV-1 cells as WT, T217E pseudo-phosphorylated and T217A non-phosphorylatable versions of 2N4R human tau. Note that by western blotting anti- tau_{pT217} labeled EGFP-tau_{WT} and EGFP-tau_{T217E}, but not EGFP-tau_{T217A}, indicating that the T217E amino acid substitution accurately mimics that structure of the tau_{pT217} epitope.

Supplementary Table 1. Clinical characterization of human autopsy brain samples

Case #	Diagnosis	Braak Stage	Age (years)	Gender	Race	Postmortem delay (hours)
1	NML	0	NA	NA	NA	NA
2	HTN vascular changes, acute ischemic injury	0	81	F	C	24
3	NML	0	73	M	C	NA
4	NML	0	64	F	C	NA
5	early AD	I-II	82	M	C	NA
6	HTN white matter vasculopathy, vascular dementia, AD	I-II	92	F	C	60
7	HTN white matter vasculopathy, vascular dementia, AD	I-II	72	M	C	40
8	HTN white matter vasculopathy, vascular dementia, AD	I-II	82	M	C	40
9	AD	III-IV	88	F	C	48
10	AD	III-IV	79	M	C	NA
11	AD and CAA	III-IV	95	M	C	24
12	AD and CAA	V-VI	93	F	C	24
13	AD	V-VI	89	M	C	NA
14	AD and CAA	V-VI	95	F	C	NA

Abbreviations:
NML = Normal
AD = Alzheimer's disease
HTN = Hypertension
FTD/MND = Frontotemporal dementia with motor neuron disease
CAA = Cerebral amyloid angiopathy
C - Caucasian

Supplementary Table 2. Primary and secondary antibodies

Name	Tag	Type	Source / Cat # / Lot #
Mouse anti-pan-tau (Tau5)	None	Monoclonal	Lester (Skip) Binder (deceased)
Rabbit anti-tau$_{pT217}$	None	Polyclonal	Abcam / ab192665 / GR3369460-4
Mouse anti-tau$_{pT231}$	None	Monoclonal	BioLegend / 828901 / B326642
Mouse anti-tau$_{pT181}$	None	Monoclonal	BioLegend / 846602 / B328986
Chicken anti-MAP2	None	Polyclonal	Abcam / ab92434 / GR3424832-2
Mouse anti-GFAP	None	Monoclonal	Thermo Fisher Scientific / MA5-12023 / VL3151991A
Mouse anti-BIN1 (clone 99D)	None	Monoclonal	Millipore / 05-449 / 3263244
Mouse anti-PSD95	None	Monoclonal	MyBioSource / MBS804156 / 1101
Mouse anti-PHF-tau (PHF1)	None	Monoclonal	Peter Davies (deceased)
Mouse anti-tau$_{pS202/pT205}$ (AT8)	None	Monoclonal	Thermo Fisher Scientific / MN1020 / XA3461673
Mouse anti-amyloid-β (6E10)	None	Monoclonal	BioLegend / 803001 / B293112
Goat anti-rabbit IgG	Alexa Fluor 488	Polyclonal	Invitrogen / A11034 / 2286890
Goat anti-mouse IgG	Alexa Fluor 488	Polyclonal	Invitrogen / A11029 / 2179204
Goat anti-chicken Igγ	Alexa Fluor 568	Polyclonal	Invitrogen / A11041 / 2306812
Goat anti-mouse IgG	Alexa Fluor 647	Polyclonal	Invitrogen / A21235 / 2284596
Goat anti-rabbit IgG	Alexa Fluor 647	Polyclonal	Invitrogen / A21244 / 2390713
Goat anti-rabbit IgG	IRDye 680	Polyclonal	LI-COR / 926-68071 / D10603-15
Goat anti-mouse IgG	IRDye 800	Polyclonal	LI-COR / 926-32210 / D10128-15

Supplementary Table 3. Human and mouse proteins containing the LPpTPP sequence

(from Phosphosite Plus:https://www.phosphosite.org/homeAction)

GENE	PROTEIN	SPECIES	ACCESSION #	MOLECULAR WEIGHT	AMINO ACID START	AMINOACID END	MODIFICATION SITES	PRESENT IN BRAIN OR NEURONS?
Atoh8	ATOH8	mouse	UP:Q99NA2	34,785	123	127	T125	Brain
CEPT1	CEPT1	human mouse	UP:Q9Y6K0 UP:Q8BGS7	46,554 46,434	38	42	T40	Both
DIDO1	DATF1	human	UP:Q9BTC0	243,873	1660	1664	T1662	Both
KMT2C	MLL3	human mouse	UP:Q8NEZ4 UP:Q8BRH4	541,370 540,187	3975 3968	3979 3972	T3977, T3970	Both
KMT2D	MLL4	human mouse	UP:O14686 UP:Q6PDK2	593,389 600,245	4680 4731	4684 4735	T4682 T4733	Both
MYC	Myc	human mouse	UP:P01106 UP:P01108	48,804 48,971	56	60	T58	Brain
MYCN	N-Myc	human mouse	UP:P04198 UP:P03966	49,561 49,572	56	60	T58	Both
Map3k14	Nik	mouse	UP:Q9WUL6	103,080	688	692	T690	Both
ZNF746	PARIS	human	UP:Q6NUN9	69,136	601	605	T603	Both
PEX12	PEX12	human	UP:O00623	40,797	279	283	T281	Brain
PHACTR3	PHACTR3	human mouse	UP:Q96KR7 UP:Q8BYK5	62,552 62,652	234 233	238 237	T236, T235	Both
POU4F1	POU4F1	human	UP:Q01851	42,697	37	41	T39	Both
PPIP5K2	PPIP5K2	human	UP:O43314	140,407	1190	1194	T1192	Both
Rab11fip5	RAB11FIP5 isoform 2	mouse	UP:Q6ZQ33	142,909	1126	1130	T1128	Both
RALGPS1	RALGPS1	human mouse	UP:Q5JS13 UP:A2AR50	62,133 65475	329	333	T331	Both
RAVER1	RAVER1 isoform 2	human mouse	UP:Q8IY67-2 UP:Q9CW46	77,860 79,382	486 492	490 496	T488, T494	Both
ESRP1	RBM35A	human mouse	UP:Q6NXG1 UP:Q6NXG1	75,585 75,549	424 423	428 427	T426, T425	Brain
MAPT	Tau	human mouse	UP:P10636 UP:P10637	78,928 76,243	532 507	536 511	T534, T509	Both
VARS1	VARS	human	UP:P26640	140,476	282	286	T284	Brain

Chapter 3: A pathway for tau_{pT217}- dependent synaptic dysfunction

ABSTRACT

Introduction: Tau phosphorylation at threonine 217 is a promising biomarker for early detection of Alzheimer's disease which was predominantly localized in the dendritic spines.
Methods: Site directed mutagenesis at T217 site to glutamic acid or alanine was performed and expressed in cultured mouse cortical and hippocampal neurons where the effect of calcium signals were monitored at different pharmological modifications.
Results: Increase in intracellular calcium signal was observed for tau_{T217E} when neurons were treated with glutamate and NMDA alone. The pattern was opposite with AMPA receptor (AMPAR) and NMDA receptor (NMDAR) inhibitors.
Conclusion: Increase in calcium signaling with stimulation of AMPAR, NMDAR and decrease with inhibition of AMPAR and NMDAR suggest that tau_{T217E} acts as a modulator of AMPAR and NMDAR which alters neuronal synapses in Alzheimer's disease (AD) brain. This work helped to propose an underlying molecular and cellular mechanisms of tau_{pT217} in altering AMPAR and NMDAR dependent neurotransmission in AD brain. Altogether, this study provides clues in understanding mechanism behind the effect of tau_{pT217}- dependent synaptic dysfunction.

Keywords: Alzheimer's disease, tau phosphorylation, dendritic spines, calcium signaling, NMDAR and AMPAR

1 | INTRODUCTION

Chapter 2 showed the physiological presence of tau_{pT217} in the dendritic spines [48]. Localization of tau_{pT217} in the dendritic spines raises its potential role in synaptic dysfunction [9] which is an index of neurotoxicity and is often associated with AD. Synaptic function in the neurons is tracked by calcium signaling. Among the multiple calcium influx sources in neurons which is an important intracellular messenger in neurons [49], glutamate type receptors, AMPA receptors (AMPARs) and NMDA receptors (NMDRs) mediate a major part of the postsynaptic calcium influx in the dendritic spines of cortical [50] and hippocampal neurons [51].

It has been proven that tau phosphorylation plays a critical role in NMDARs dependent neurotoxicity [52]. Therefore, to understand the functional relevance of tau_{pT217} in the dendritic spines and to support the notion whether tau phosphorylation at T217 affects AMPARs or NMDARs or both dependent neurotransmission, I proposed a pathway on how tau_{pT217} targets the postsynaptic compartment of excitatory synapses and, specifically, AMPA and NMDA receptors which in turn could contribute to the impaired glutamatergic neurotransmission observed in AD.

In accordance with the above background, my first step was to design and create neuron specific green fluorescent tagged wild type 2N4R tau. To mimic phosphorylation, T217 in 2N4R tau was mutated to glutamic acid (E) and, as a non-phosphorylation control, to

alanine (A) individually. The three different tau constructs were then expressed in mouse cortical and hippocampal neurons via lenti-viral transduction. I then performed calcium imaging to track synaptic activity with and without treating the tau knockout mouse cortical neurons at DIV-21 and wild type mouse hippocampal neurons at DI-16 with different pharmacological modulators.

By doing so, I observed an increase in intracellular calcium signals in mouse cultures with T217E compared to WT tau form when treated individually with glutamate and NMDA. The result was opposite with AMPAR and NMDAR inhibitors. Taken together, my data showed for the first time that tau phosphorylation at T217 in the dendritic spines is involved in synaptic dysfunction by modulating AMPAR and NMDAR dependent neurotransmission.

2 | METHODS

2.1 | Fluorescent fusion neuron specific plasmids

2N4R tau tagged with EGFP was inserted at the C-terminal site of the background vector pHR-hSyn-EGFP (Addgene, catalog# 114215) between BamHI and NcoI restriction sites. The sequence was validated by Sanger sequencing. To mimic phosphorylation, T217 in 2N4R tau (wild type) were mutated to glutamic acid (E) and, as a non-phosphorylation control, to alanine (A) individually. Validation of tau mutants were confirmed by digestion, sequencing of the plasmids and expression of the plasmids in mouse tau knockout neurons.

2.2 | Lentivirus production and infection

Lentiviruses were prepared as previously described [53] with some modifications. Briefly, HEK293T/17 cells were plated on 150 mm dishes until they reached 60-70% confluency. The cells then received a full media change using Opti-MEM lentiviral packaging reduced growth serum. The next day, the cells were transfected with 15 μg total plasmid DNA at a ratio of expression/shRNA vector (50%), packaging (pspax2) (37.5%) and envelope (pMD2.G) (12.5%) vectors, with 30 μl each of P3000 Reagent and Lipofectamine 3000TM Reagent (ThermoFisher Scientific). Packing (pspax2) and envelope (pMD2.G) vectors were obtained from Addgene. After 24 hour and 52 hour the lentiviral containing media were collected and stored at 4°C. The lentiviral containing media were then concentrated by centrifugation at 23,000 rpm for 2 hour at 4°C using a Beckman SW28 swinging bucket rotor. Transduction efficiency was monitored by immunoblot and immunofluorescence.

2.3 | Western Blotting

Mouse cultured neurons were lysed using N-PER™ Neuronal Protein Extraction Reagent. Samples were resolved by SDS-PAGE using 10% acrylamide/bis-acrylamide gels and transferred to 0.2 μm nitrocellulose (Bio-Rad). Membranes were blocked with Odyssey blocking buffer (LI-COR) and were incubated with primary antibodies and secondary IRDye-labeled antibodies (Table 1) diluted into Odyssey blocking buffer. After each antibody step, the blots were washed five times in PBS/0.1% Tween 20. The blots were

then imaged using BioRad ChemiDoc MP. Information for primary and secondary antibodies are shown in Table 1.

2.4 | Microscopy

Primary mouse hippocampal neuron cultures were prepared from dissected brain cortices of pup0 wild-type (WT) C57/Bl6 mice and cortical neuron cultures from E16-18 tau knockout (TKO) mice in the same background strain and were maintained in Neurobasal medium supplemented with B27. All experiments were completed after neurons had been in culture for a total of 16-21days. Animals were maintained, bred and euthanized in compliance with all policies of the Animal Care and Use Committee of the University of Virginia.

Mouse neurons were washed with PBS following fixation for 5 minutes with methanol at -20º C. The neurons were incubated with blocking solution (PBS with 5% bovine serum albumin and x% Triton X-100) for 1 hour, followed by sequential incubations for 30-60 minutes each with primary and secondary antibodies. Multiple washes with PBS were followed in each antibody step, and immediately prior to being sealed with a coverslip using Fluoromount G with Hoechst 33342 (ThermoFisher catalog # 62249), cultures were washed for 10 minutes. Immunofluorescence was performed to validate the synapsis at DIV-21 and DIV-16 for tau knockout mouse cortical neurons and wild type mouse hippocampal neurons, respectively.

See Supplementary Table 1 for descriptions of all antibodies used for immunofluorescence and western blotting.

For live cell imaging, the tau knockout mouse cortical neurons and wild type mouse hippocampal neuron cultures were washed 3 times with DMEM, Phenol Red free, and treated with Cal-590™ AM (AAT Bioquest, Inc, 20510) was diluted in DMEM, Phenol Red free in 1: 1000 dilution factor for 30 min at 37°C and 5% oxygen and 5% CO2 and live imaging was performed under 40 X Zeiss 980 confocal microscope for 250 milliseconds in Keck Center at the University of Virginia. Live cell imaging was also performed after treating the neurons with different pharmacologic modulators, AMPAR agonist, glutamate (100 µM, Sigma-Aldrich, catalog# G1251); NMDAR agonist, NMDA (100 µM, Millipore Sigma, catalog# M3262); AMPAR inhibitor, CNQX (10 µM, Abcam, catalog# ab120017) and NMDAR inhibitor, MK-801 (10 µM, Sigma-Aldrich, catalog# M107-5MG). Concentrations for glutamate and NMDA was selected according to other group [52] and concentrations for CNQX and MK-801 was selected following the protocol from the Bloom's lab [54]. Cultured neurons were exposed to drugs for ~5-10 minutes before being processed calcium imaging.

See Supplementary Table 2 for descriptions of all compounds used for the study.

For calcium influx quantification, the maximal fluorescence increase (ΔF) was normalized to the baseline fluorescence (F0). The ΔF/F0 ratio after drug treatment was divided by the ΔF/F0 ratio before drug treatment.

3 | RESULTS

3.1 | Validation of T217E pseudo-phosphorylation in TKO mouse cortical neurons

Three forms of tau-EGFP with respect to the tau sequence were used in the study: WT, pseudo-phosphorylated T217E and non-phosphorylatable T217A (Figure 1). To verify that the T217E amino acid substitution structurally mimics tau_{pT217}, I used western blotting with anti-tau_{pT217} of TKO mouse cortical neurons transduced to express tau-$EGFP_{WT}$, tau-$EGFP_{T217E}$ and tau-$EGFP_{T217A}$, the latter of which cannot be phosphorylated at position 217 because of the alanine mutation at that site. As shown in Figure 1, anti- tau_{pT217} recognized tau-$EGFP_{WT}$ and tau-$EGFP_{T217E}$, but not tau-$EGFP_{T217A}$. The immunoreactivity with tau-$EGFP_{WT}$ reflects a baseline level of WT tau phosphorylation of T217. The robust immunoreactivity of anti-tau_{pT217} with tau-$EGFP_{T217E}$ and the absence of immunoreactivity with tau-$EGFP_{T217A}$ demonstrates that the T217E mutation structurally mimics phosphorylation of T217.

3.2 | Mouse cortical cultures at DIV-21 and hippocampal cultures at DIV-16 are synaptically matured

To demonstrate if the cultured TKO mouse cortical neurons at DIV-21 and WT mouse hippocampal neurons at DIV-16 are synaptically active, I performed immunofluorescence by triple-labeling the cultures with anti-AMPAR, anti-NMDAR separately with either anti-synaptophysin (presynaptic marker) or anti-PSD95 (postsynaptic marker) and MAP2 (neuronal marker) antibodies (Supplementary Figures 1, 2). I also double-labeled the cultures with anti-synaptophysin and anti-PSD95 antibodies. As shown in Supplementary Figure 3, strong colocalization was observed between presynaptic and postsynaptic markers with a Pearson correlation coefficient of ~ 0.3. This concludes that mouse cortical neurons and mouse hippocampal neurons are matured enough to show synaptic activity at DIV-21 and DIV-16 respectively.

3.3 | Tau_{pT217} mediates AMPA and NMDA receptors dependent neurotransmission in mouse cortical and hippocampal neurons

To test the hypothesis that tau phosphorylation at T217 modulates AMPAR or NMDAR dependent neurotransmission, I expressed three forms of human 2N4R tau-EGFP, WT, pseudo-phosphorylated T217E and non-phosphorylatable T217A in TKO mouse cortical neurons (Figure 2 shows results from Tau-$EGFP_{(T217E)}$) and WT mouse hippocampal neurons (Figure 3), and performed calcium imaging at DIV-21 for cortical neurons and at DIV-16 for hippocampal neurons after treating each conditions individually with calcium dye for ~30 mins. Intracellular calcium signals were recorded from the neurons before any pharmacological modulation. This was followed by treatment with 10 µM AMPAR inhibitor and 10 µM NMDAR inhibitor prior to the treatment with 100 µM glutamate and 100 µM NMDA, respectively. Calcium signals were also recorded in neurons treated with only NMDA or glutamate.

As shown in Figure 2 and Figure 3, increase in calcium influx was observed with both AMPA and NMDA receptor agonists in tau-EGFP$_{T217E}$. The effect was opposite with AMPA and NMDA receptor inhibitors. This concludes that tau phosphorylation at T217 modulate both AMPAR and NMDAR-dependent neurotransmission.

4 | DISCUSSION

As an extension to chapter 2 which provided a clue on role of tau$_{pT217}$ in synaptic dysfunction, in chapter 3, I performed calcium imaging to study the effect of tau phosphorylation at T217 on neurotransmission expressing tau-EGFP. While further work is required, from the data that I have so far, using conventional confocal microscopy, I found that tau-EGFP pseudo-phosphorylated at position 217 by a T-to-E amino acid substitution increases intracellular calcium signals than WT tau coupled to EGFP by modulating both AMPA and NMDA receptors. In contrast, the calcium signal was low with AMPAR and NMDAR inhibitors.

Through this study, I proposed a pathway showing that tau phosphorylation at T217 causes increase in intracellular calcium levels which allows tau$_{pT217}$ to mediate AMPARs and NMDARs dependent neurotransmission similar to cellular prion proteins (Figure 4). Co-operative activity of AMPARs and NMDARs are closely associated with cognitive impairment in AD [55]. Any imbalance between AMPA and NMDA receptors alters neurotransmission which might eventually lead to synaptopathy. Correlating the effect of tau phosphorylation with cognitive function in AD further provides evidence on using tau$_{pT217}$ as a promising diagnostic and potential therapeutic target.

Although further work is required to understand what and how tau$_{pT217}$ causes synaptic dysfunction, my findings are first of its kind. Further expanding my work by behavioral and physiological studies could contribute in refining the optimal pathway for AD pathogenesis.

FIGURE LEGENDS

FIGURE 1 Tau-EGFP variants used for calcium imaging. The fluorescent fusion proteins were expressed in 8 days old tau knockout mouse cortical neurons as WT, T217E pseudo-phosphorylated and T217A non- phosphorylatable versions of 2N4R human tau. Note that by western blotting anti- tau$_{pT217}$ labeled tau-EGFP$_{WT}$ and tau-EGFP$_{T217E}$, but not tau-EGFP$_{T217A}$, indicating that the T217E amino acid substitution accurately mimics that structure of the tau$_{pT217}$ epitope.

FIGURE 2 Tau phosphorylation at T217 increases calcium signal by mediating AMPA and NMDA receptors in tau knockout mouse cortical neurons. The maximal fluorescence increase (ΔF) was normalized to the baseline fluorescence (F0). The ΔF/F0 ratio after drug treatment was divided by the ΔF/F0 ratio before drug treatment.

FIGURE 3 Tau phosphorylation at T217 increases calcium signal by mediating AMPA and NMDA receptors in wild type mouse hippocampal neurons. The maximal fluorescence

increase (ΔF) was normalized to the baseline fluorescence (F0). The ΔF/F0 ratio after drug treatment was divided by the ΔF/F0 ratio before drug treatment.

FIGURE 4 A proposed pathway for AMPAR and NMDAR dependent neurotransmission which eventually leads to synaptic dysfunction by tau phosphorylation at T217 similar to cellular prion protein.

SUPPLEMENTARY MATERIAL LEGENDS

Supplementary Figure 1 Validation of synapsis by immunofluorescence in cultured TKO mouse cortical neurons at DIV-21. Neurons were triple-labeled with anti-AMPAR and anti-NMDAR separately with either anti-synaptophysin (neuronal presynaptic marker) or anti-PSD95 (post-synaptic marker) and anti-MAP2 (neuronal marker) antibodies. Single plane confocal images are shown.

Supplementary Figure 2 Validation of synapsis by immunofluorescence in cultured WT mouse hippocampal neurons at DIV-16. Neurons were triple-labeled with anti-AMPAR and anti-NMDAR separately with either anti-synaptophysin (neuronal presynaptic marker) or anti-PSD95 (post-synaptic marker) and anti-MAP2 (neuronal marker) antibodies. Single plane confocal images are shown.

Supplementary Figure 3 Tau knockout mouse cortical neurons at DIV-21 and wild type mouse hippocampal neurons at DIV-16 are synaptically matured. Cultured mouse neurons were double-labeled anti-synaptophysin (presynaptic marker) and anti-PSD95 (post-synaptic marker). Single plane confocal images are shown. Pearson correlation coefficients was used for quantifying co-localization.

Supplementary Table 1 Primary and secondary antibodies used in the study.

Supplementary Table 2 Compounds used in the study.

FIGURES

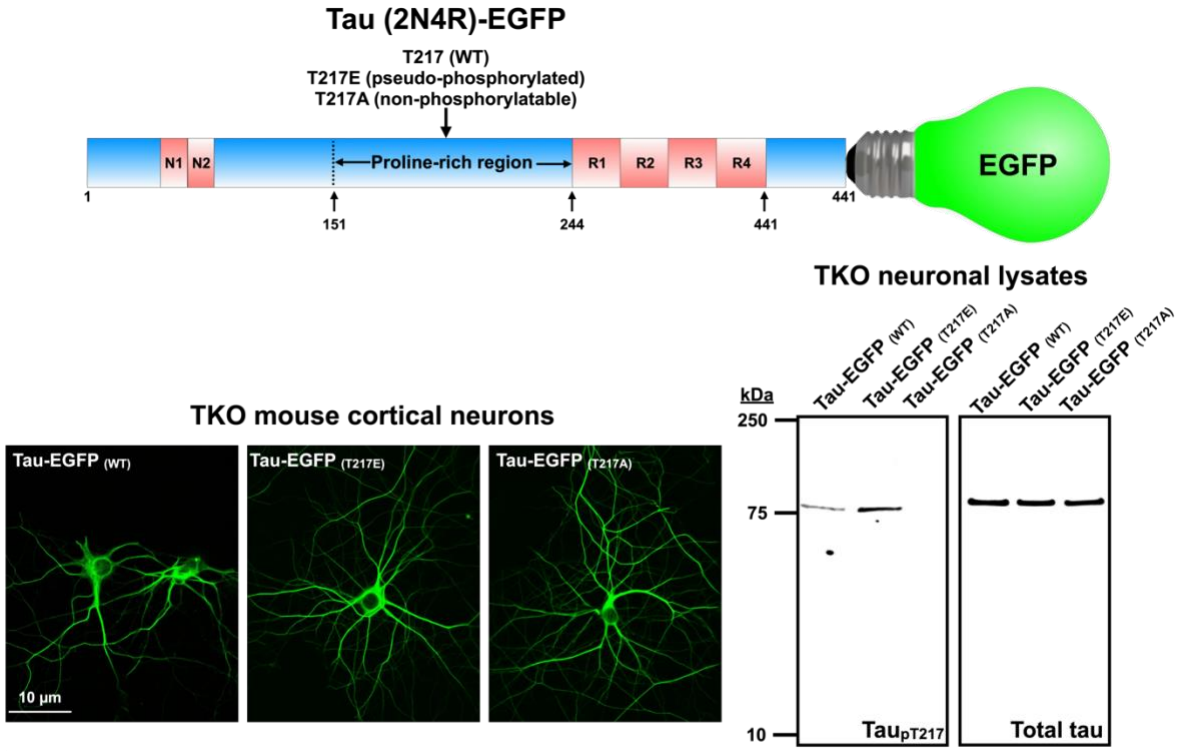

FIGURE 1 Tau-EGFP variants used for calcium imaging.The fluorescent fusion proteins were expressed in 8 day old tau knockout mouse cortical neurons as WT, T217E pseudo-phosphorylated and T217A non- phosphorylatable versions of 2N4R human tau. Note that by western blotting anti- tau_{pT217} labeled tau_{WT}-EGFP and tau_{T217E}-EGFP, but not tau_{T217A}-EGFP, indicating that the T217E amino acid substitution accurately mimics that structure of the tau_{pT217} epitope.

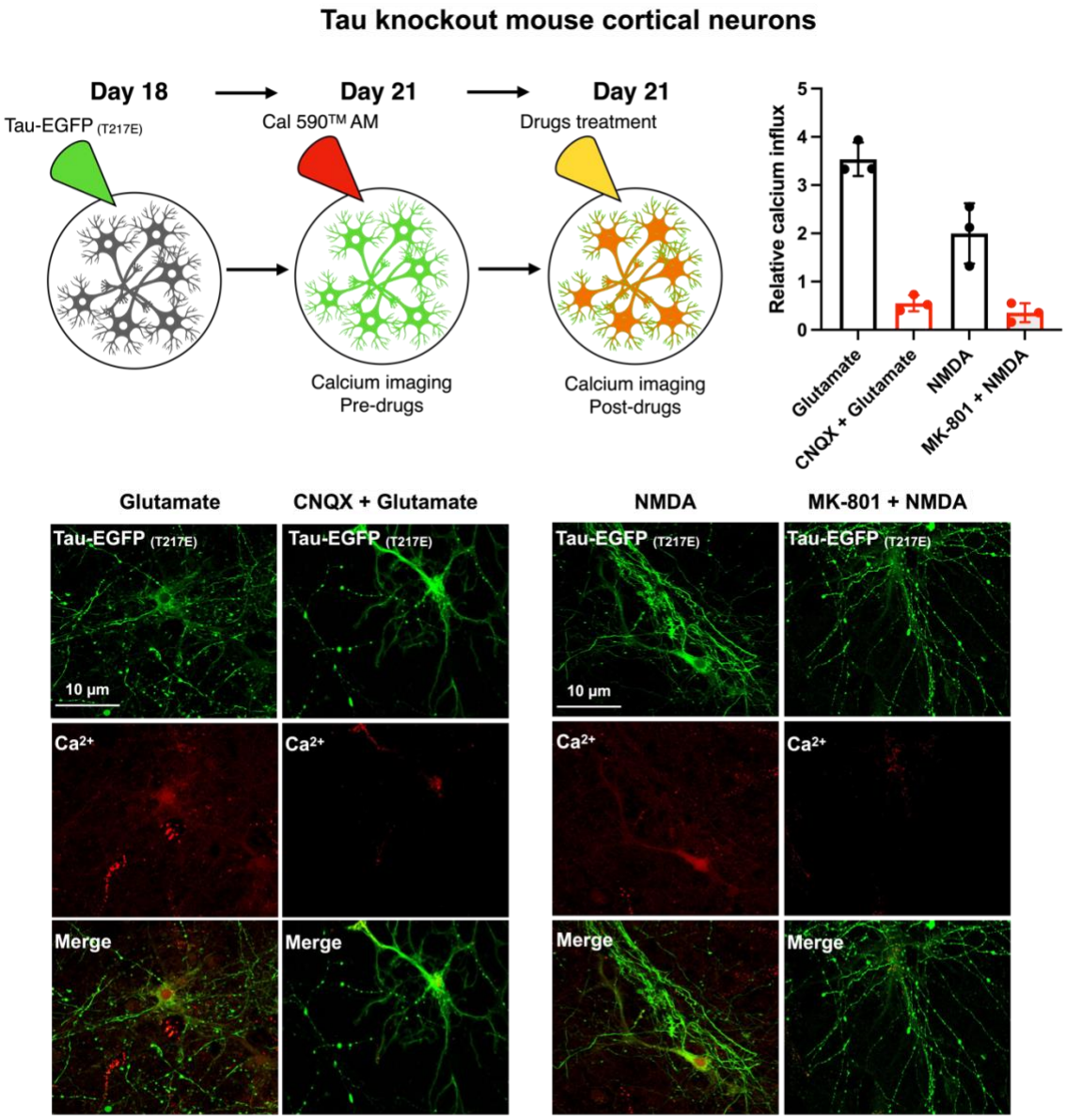

FIGURE 2 Tau phosphorylation at T217 increases calcium signal by mediating AMPA and NMDA receptors in tau knockout mouse cortical neurons. The maximal fluorescence increase (ΔF) was normalized to the baseline fluorescence (F0). The ΔF/F0 ratio after drug treatment was divided by the ΔF/F0 ratio before drug treatment.

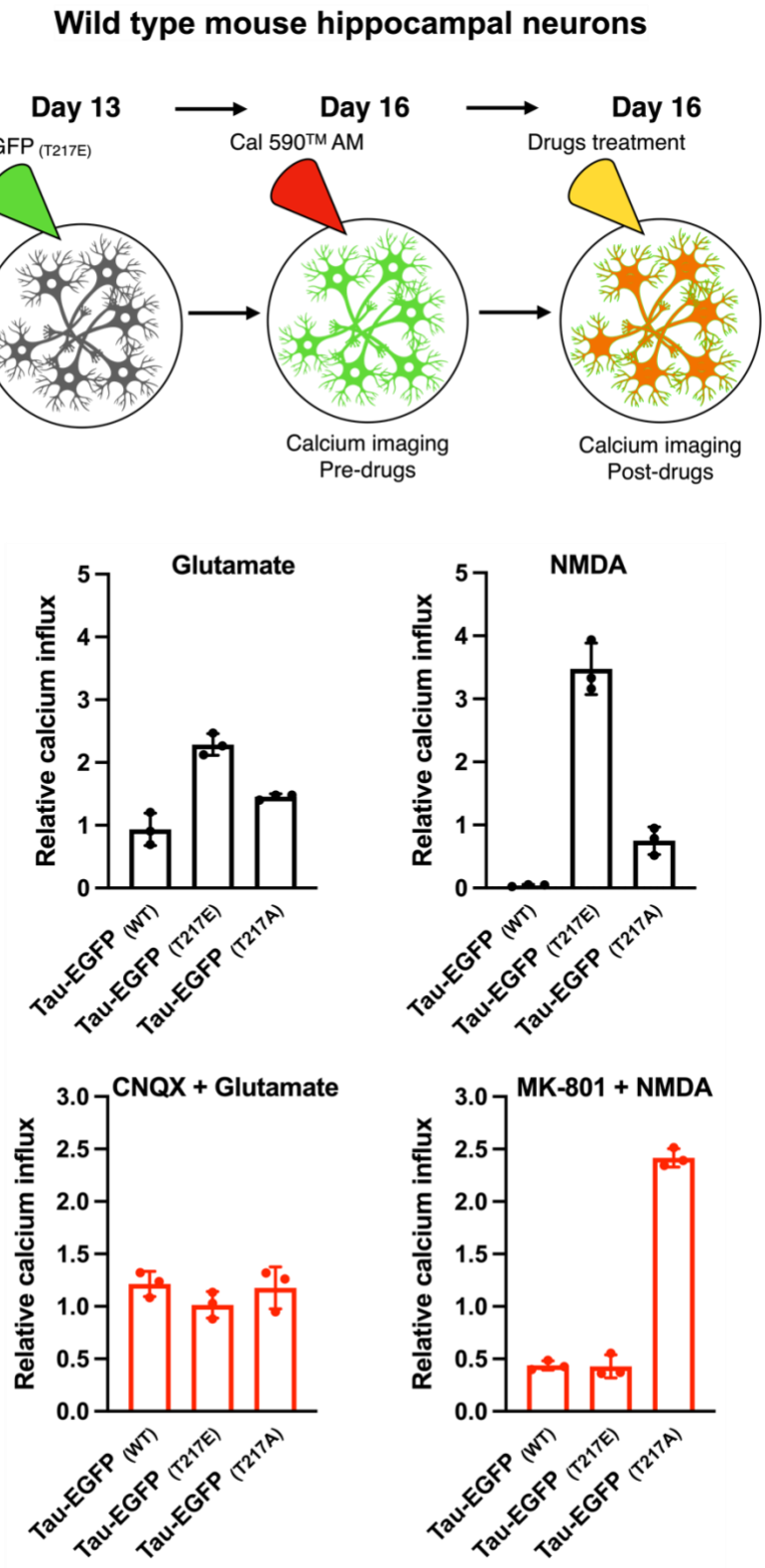

FIGURE 3 Tau phosphorylation at T217 increases calcium signal by mediating AMPA and NMDA receptors in wild type mouse hippocampal neurons. The maximal fluorescence increase (ΔF) was normalized to the baseline fluorescence (F0). The ΔF/F0 ratio after drug treatment was divided by the ΔF/F0 ratio before drug treatment.

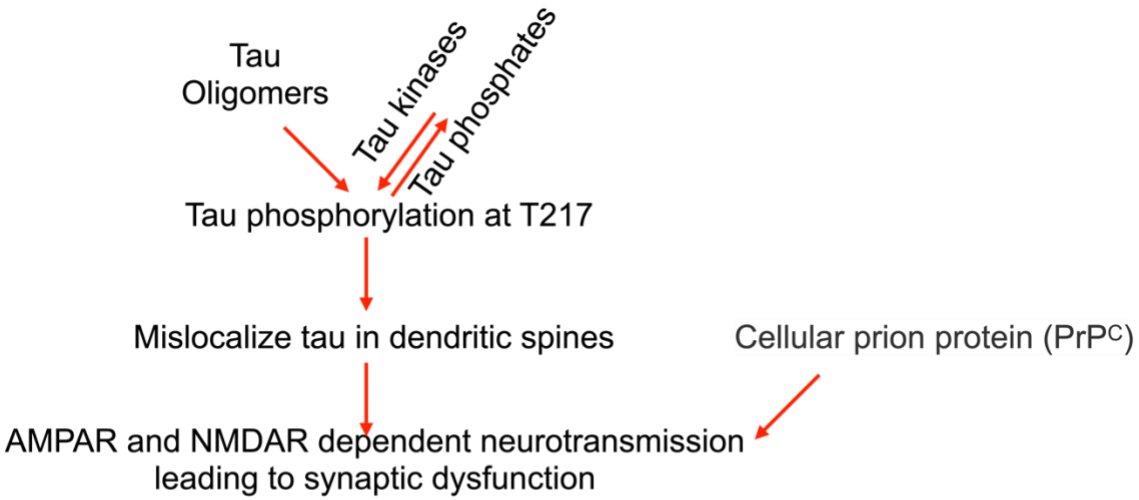

FIGURE 4 A proposed pathway for AMPAR and NMDAR dependent neurotransmission which eventually leads to synaptic dysfunction by tau phosphorylation at T217 similar to cellular prion protein.

SUPPLEMENTARY MATERIALS

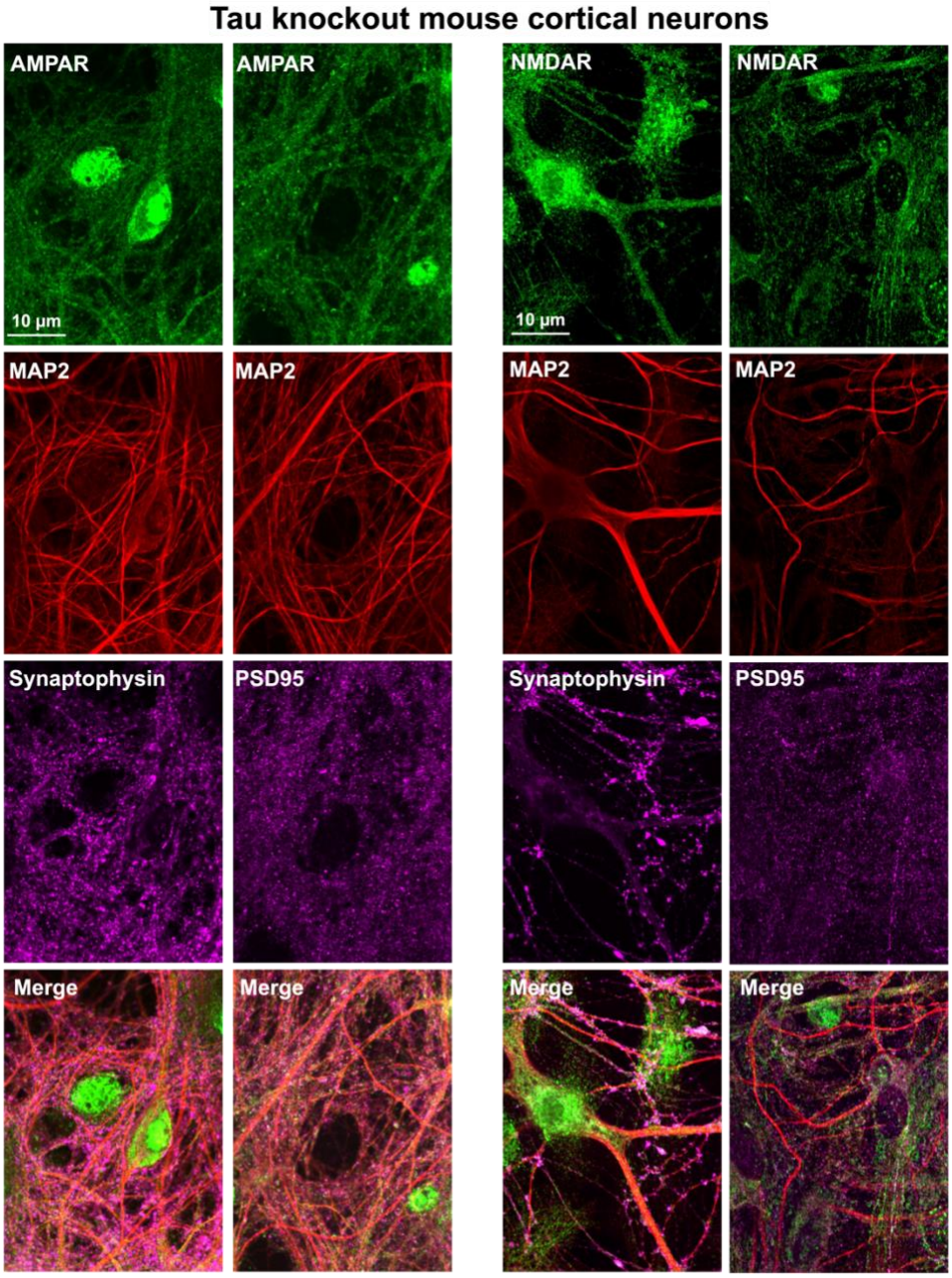

Supplementary Figure 1 Validation of synapsis by immunofluorescence in cultured TKO mouse cortical neurons at DIV-21. Neurons were triple-labeled with anti-AMPAR and anti-NMDAR separately with either anti-synaptophysin (neuronal presynaptic marker) or anti-PSD95 (post-synaptic marker) and anti-MAP2 (neuronal marker) antibodies. Single plane confocal images are shown.

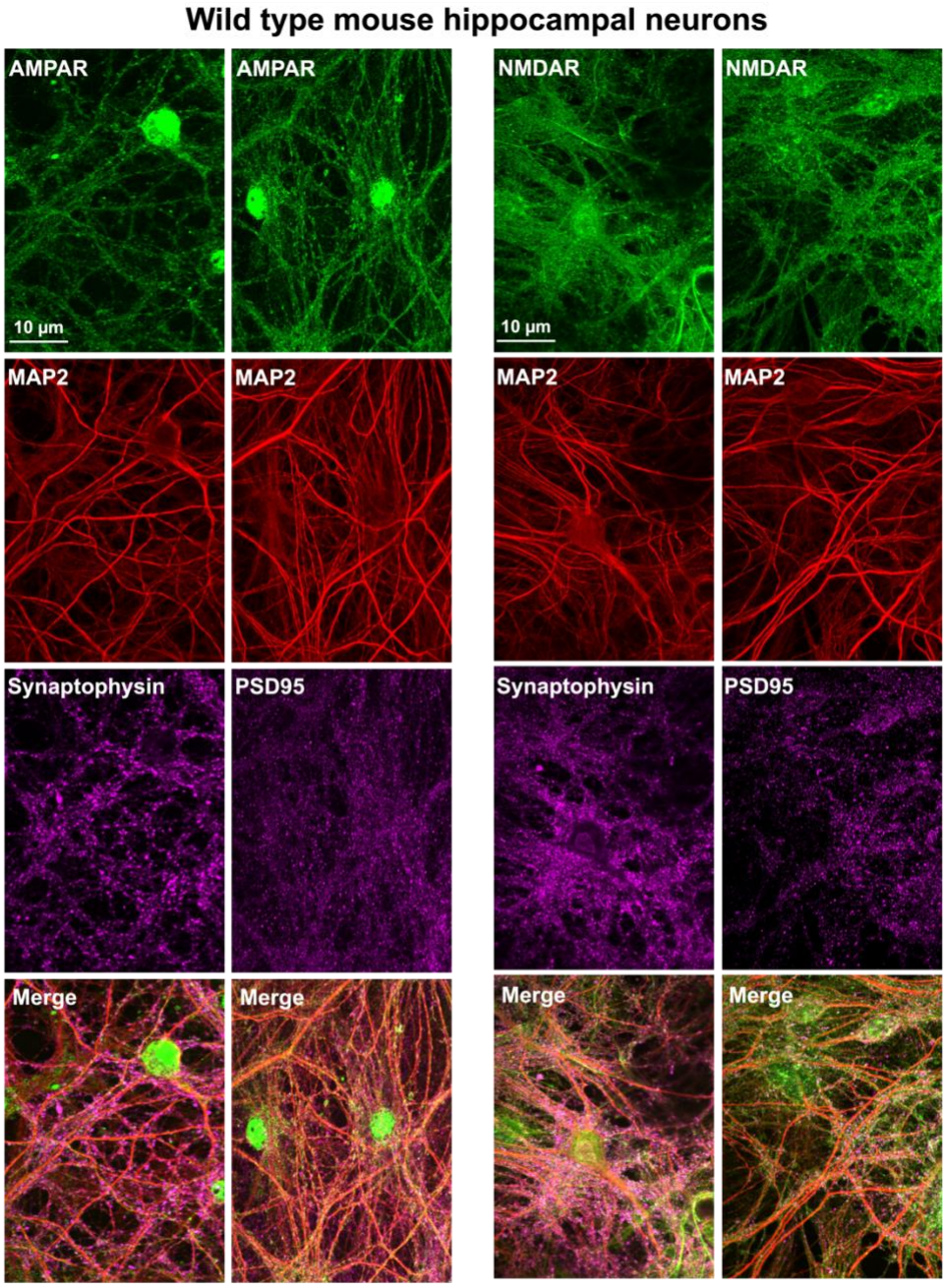

Supplementary Figure 2 Validation of synapsis by immunofluorescence in cultured WT mouse hippocampal neurons at DIV-16. Neurons were triple-labeled with anti-AMPAR and anti-NMDAR separately with either anti-synaptophysin (neuronal presynaptic marker) or anti-PSD95 (post-synaptic marker) and anti-MAP2 (neuronal marker) antibodies. Single plane confocal images are shown.

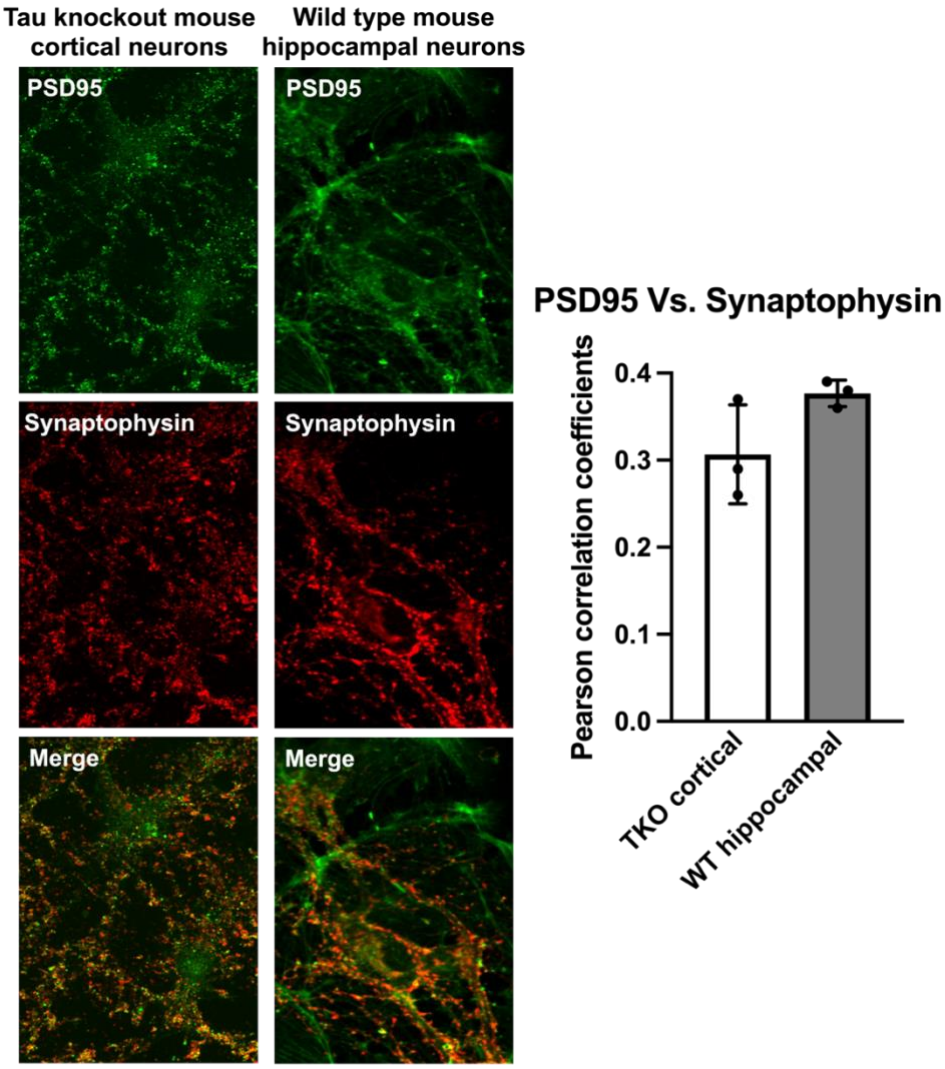

Supplementary Figure 3 Tau knockout mouse cortical neurons at DIV-21 and wild type mouse hippocampal neurons at DIV-16 are synaptically matured. Cultured mouse neurons were double-labeled anti-synaptophysin (presynaptic marker) and anti-PSD95 (post-synaptic marker). Single plane confocal images are shown. Pearson correlation coefficients was used for quantifying co-localization.

Supplementary Table 1. Primary and secondary antibodies

Name	Tag	Type	Source / Cat #/ Lot #
Mouse anti-pan-tau (Tau5)	None	Monoclonal	Lester (Skip) Binder (deceased)
Rabbit anti-tau$_{pT217}$	None	Polyclonal	Abcam / ab192665 / GR3369460-4
Chicken anti-MAP2	None	Polyclonal	Abcam / ab92434 / GR3424832-2
Mouse anti-PSD95	None	Monoclonal	MyBioSource / MBS804156 / 1101
Rabbit anti-PSD95	None	Polyclonal	Invitrogen / 51-6900 / XC-346008
Mouse anti-synaptophysin	None	Monoclonal	Santa Cruz Biotechnology / sc-17750 / C1022
Rabbit anti-NMDAR	None	Polyclonal	Invitrogen / PA3-102 / XD352526
Rabbit anti-AMPAR	None	Monoclonal	Cell Signaling / 13607S / 2
Goat anti-rabbit IgG	Alexa Fluor 488	Polyclonal	Invitrogen / A11034 / 2286890
Goat anti-chicken Igγ	Alexa Fluor 568	Polyclonal	Invitrogen / A11041 / 2306812
Goat anti-mouse IgG	Alexa Fluor 647	Polyclonal	Invitrogen / A21235 / 2284596
Goat anti-rabbit IgG	IRDye 680	Polyclonal	LI-COR / 926-68071 / D10603-15
Goat anti-mouse IgG	IRDye 800	Polyclonal	LI-COR / 926-32210 / D10128-15

Supplementary Table 2. Compounds used in the study

Compound	Solvent of Stock	Source/Cat no.
AMPAR agonist, Glutamate, 100 μM	100 mg/ml, 1 M HCl	Sigma-Aldrich/G1251
NMDAR agonist, NMDA, 100 μM	50 mg/ml, H20	Sigma-Aldrich/6384-92-5
AMPAR inhibitor, CNQX, 10 μM	100 mM, DMSO	Abcam/ab120017
NMDAR inhibitor, MK-801, 10 μM	6 mg/ml, H20	Sigma-Aldrich/M107-5MG

Chapter 4: Future directions for tau$_{pT217}$ in Alzheimer's disease research

Currently there are no FDA approved drugs for AD that targets tau. The current AD drugs that have been FDA approved either act through mechanisms such as targeting amyloid or prevent butyrylcholine/ acetylcholine breakdown in the brain or antagonize NMDA receptors. A tabular form of the mechanism of action of the different FDA approved drugs for AD are shown in Table 1 of chapter 1.

Several past clinical trials targeting amyloid have failed which has challenged the hypothesis that amyloid accumulation is the initial step in AD pathogenesis and emphasizing the immediate need for novel therapies and promising targets. Since tau has been found to play a much more important role in AD than targeting amyloid, I hope that in the future we are able to find drugs that delay AD progression by targeting tau. This can be done by exploring different hypotheses regarding tau's role in AD including its interaction with microglial cells, prion/misfolding hypothesis, tau aggregation, microtubule stabilization, and dephosphorylation of tau. It remains to be seen how promising the results of the ongoing clinical trials will be.

Understanding the localization and functional role of tau$_{pT217}$ is an initial step that provides clues to new approaches towards therapies and early diagnosis techniques for AD. Findings from chapter 2 and 3 provided vital evidence in future work that could help target tau$_{pT217}$ to develop AD drugs with precision.

Tau$_{pT217}$ mislocalization to the dendritic spines provides an interesting clue about their roles in synaptic function and/or other biochemical processes within neurons. Tau phosphorylation at T217 mediating NMDA and AMPA receptors dependent neurotransmission provided a direct clue that blockage of tau phosphorylation at T217 may be excitoprotective, particularly in pathological conditions associated with an abnormal accumulation of tau. Weak MT binding of tau$_{pT217}$ implies that destabilization of MT after tau phosphorylation at T217 could contribute to neurotoxicity. Further, the abundance of intracellular tau$_{pT217}$ levels induced by xcTauOs but not by xcAβOs offered new therapeutic opportunities in AD and other neurodegenerative diseases associated with tau pathology.

As future steps, my discovery could be extended by comparing binding affinity of all three phospho-tau epitopes (T181, T217 and T231) with microtubules and determining the optimal tau variants. For this, we can create EGFP-tagged tau variants (T181 and T231) with non-neuron specific promoters and perform FRAP and FRET microscopy.

We can also extend the findings of NMDA and AMPA receptor dependent neurotransmission effects of phospho-tauT217 by performing behavioral studies in mice. Through behavioral studies, we can examine the working and long-term memories. For this, we can stereotaxically inject AAV mediated EGFP-tagged versions of all three phospho-tau epitopes in the hippocampus of wild type mice. By doing so, we can identify the most pathological form of phospho-tau variants to detect AD early on. Based on the identified optimal phospho-tau variant, we can investigate the upstream/downstream mechanisms.

In the future, a biochemical therapeutic strategy can be developed to stabilize microtubules by protecting tau from being phosphorylated at the optimal site. This strategy could eventually avoid neuronal deformation and delay or treat the progression of AD.

Another future direction could be comparing the effect of all kinases and phosphatases that activate the three phospho-tau epitopes. There are 11 kinases that act on tau_{pT181}, 11 kinases that act on tau_{pT217} and 13 kinases that act on tau_{pT231}. However, we still don't know the type of phosphatases that dephosphorylate tau at those three epitopes. My hope is to be able to identify an optimal kinase and optimal phosphatase for tau. Joining these pieces together, the ultimate goal would be designing a "molecular spring" that could maintain the activity of kinase and phosphatase in balance and could stop hyperphosphorylation of tau. Further, we can also design a "molecular cap" to prevent tau phosphorylation at the optimal phospho-tau epitope.

Overall, my PhD project provides clues for different functional roles of tau_{pT217} and other isoforms of phosphorylated tau in AD. The findings from my PhD project are a step towards exploring tau_{pT217} as a potential molecular therapeutic target for AD which might lead to new therapies or early diagnostic techniques in the future.

REFERENCES

[1]Tarawneh R, Holtzman DM. The clinical problem of symptomatic Alzheimer disease and mild cognitive impairment. Cold Spring Harbor perspectives in medicine. 2012;2(5):a006148.
[2]Cvetković-Dožić D, Skender-Gazibara M, Dožić S. Neuropathological hallmarks of Alzheimer's disease. Archive of Oncology. 2001;9(3):195-9.
[3]Gaugler J, James B, Johnson T, Reimer J, Solis M, Weuve J, et al. 2022 Alzheimer's disease facts and figures. ALZHEIMERS & DEMENTIA. 2022;18(4):700-89.
[4]Shaw LM, Korecka M, Clark CM, Lee VM-Y, Trojanowski JQ. Biomarkers of neurodegeneration for diagnosis and monitoring therapeutics. Nature reviews Drug discovery. 2007;6(4):295-303.
[5]Nykamp MJ, Zorumski CF, Reiersen AM, Nicol GE, Cirrito J, Lenze EJ. Opportunities for Drug Repurposing of Serotonin Reuptake Inhibitors: Potential Uses in Inflammation, Infection, Cancer, Neuroprotection, and Alzheimer's Disease Prevention. Pharmacopsychiatry. 2022;55(01):24-9.
[6]Ancidoni A, Bacigalupo I, Remoli G, Lacorte E, Piscopo P, Sarti G, et al. Anticancer drugs repurposed for Alzheimer's disease: a systematic review. Alzheimer's Research & Therapy. 2021;13(1):1-15.
[7]Sulsenti R, Frossi B, Bongiovanni L, Cancila V, Ostano P, Fischetti I, et al. Repurposing of the Antiepileptic Drug Levetiracetam to Restrain Neuroendocrine Prostate Cancer and Inhibit Mast Cell Support to Adenocarcinoma. Frontiers in immunology. 2021;12:563.
[8]Weingarten MD, Lockwood AH, Hwo S-Y, Kirschner MW. A protein factor essential for microtubule assembly. Proceedings of the National Academy of Sciences. 1975;72(5):1858-62.
[9]Hoover BR, Reed MN, Su J, Penrod RD, Kotilinek LA, Grant MK, et al. Tau mislocalization to dendritic spines mediates synaptic dysfunction independently of neurodegeneration. Neuron. 2010;68(6):1067-81.
[10]Lee VM, Goedert M, Trojanowski JQ. Neurodegenarative tauopathies. Annual review of neuroscience. 2001;24:1121.
[11]Derisbourg M, Leghay C, Chiappetta G, Fernandez-Gomez F-J, Laurent C, Demeyer D, et al. Role of the Tau N-terminal region in microtubule stabilization revealed by newendogenous truncated forms. Scientific reports. 2015;5(1):1-10.
[12]He HJ, Wang XS, Pan R, Wang DL, Liu MN, He RQ. The proline-rich domain of tau plays a role in interactions with actin. BMC cell biology. 2009;10(1):1-12.
[13]Khan SS, Bloom GS. Tau: the center of a signaling nexus in Alzheimer's disease. Frontiers in Neuroscience. 2016;10:31.
[14]Janelidze S, Mattsson N, Palmqvist S, Smith R, Beach TG, Serrano GE, et al. Plasma P-tau181 in Alzheimer's disease: relationship to other biomarkers, differential diagnosis, neuropathology and longitudinal progression to Alzheimer's dementia. Nature medicine. 2020;26(3):379-86.
[15]Palmqvist S, Janelidze S, Quiroz YT, Zetterberg H, Lopera F, Stomrud E, et al. Discriminative accuracy of plasma phospho-tau217 for Alzheimer disease vs other neurodegenerative disorders. Jama. 2020;324(8):772-81.

[16]Ashton NJ, Pascoal TA, Karikari TK, Benedet AL, Lantero-Rodriguez J, Brinkmalm G, et al. Plasma p-tau231: a new biomarker for incipient Alzheimer's disease pathology. Acta neuropathologica. 2021;141(5):709-24.
[17]Wennström M, Janelidze S, Nilsson KPR, Serrano GE, Beach TG, Dage JL, et al. Cellular localization of p-tau217 in brain and its association with p-tau217 plasma levels. Acta neuropathologica communications. 2022;10(1):1-12.
[18]Moloney CM, Labuzan SA, Crook JE, Siddiqui H, Castanedes-Casey M, Lachner C, et al. Phosphorylated tau fluid biomarker sites recognize earlier neurofibrillary tangle maturity levels in the postmortem Alzheimer's disease brain. bioRxiv. 2021.
[19]Dubois B, Feldman HH, Jacova C, DeKosky ST, Barberger-Gateau P, Cummings J, et al. Research criteria for the diagnosis of Alzheimer's disease: revising the NINCDS–ADRDA criteria. The Lancet Neurology. 2007;6(8):734-46.
[20]Dubois B, Feldman HH, Jacova C, Hampel H, Molinuevo JL, Blennow K, et al. Advancing research diagnostic criteria for Alzheimer's disease: the IWG-2 criteria. The Lancet Neurology. 2014;13(6):614-29.
[21]Jack Jr CR, Albert MS, Knopman DS, McKhann GM, Sperling RA, Carrillo MC, et al. Introduction to the recommendations from the National Institute on Aging-Alzheimer's Association workgroups on diagnostic guidelines for Alzheimer's disease. Alzheimer's & dementia. 2011;7(3):257-62.
[22]Holtzman DM. CSF biomarkers for Alzheimer's disease: current utility and potential future use. Neurobiology of aging. 2011;32:S4-S9.
[23]Blennow K. CSF biomarkers for Alzheimer's disease: use in early diagnosis and evaluation of drug treatment. Expert review of molecular diagnostics. 2005;5(5):661-72.
[24]Palmqvist S, Tideman P, Cullen N, Zetterberg H, Blennow K, Dage JL, et al. Prediction of future Alzheimer's disease dementia using plasma phospho-tau combined with other accessible measures. Nature Medicine. 2021;27(6):1034-42.
[25]Moussaed M, Huc-Brandt S, Cubedo N, Silhol M, Murat S, Lebart M-C, et al. Regenerating islet-derived 1α (REG-1α) protein increases tau phosphorylation in cell and animal models of tauopathies. Neurobiology of disease. 2018;119:136-48.
[26]Kandimalla R, Manczak M, Yin X, Wang R, Reddy PH. Hippocampal phosphorylated tau induced cognitive decline, dendritic spine loss and mitochondrial abnormalities in a mouse model of Alzheimer's disease. Human molecular genetics. 2018;27(1):30-40.
[27]Neddens J, Temmel M, Flunkert S, Kerschbaumer B, Hoeller C, Loeffler T, et al. Phosphorylation of different tau sites during progression of Alzheimer's disease. Acta neuropathologica communications. 2018;6(1):1-15.
[28]Clodfelder-Miller BJ, Zmijewska AA, Johnson GV, Jope RS. Tau is hyperphosphorylated at multiple sites in mouse brain in vivo after streptozotocin-induced insulin deficiency. Diabetes. 2006;55(12):3320-5.
[29]Kovacs GG, Gelpi E. Clinical Neuropathology Practice News 3-2012: the "ABC" in AD–revised and updated guideline for the neuropathologic assessment of Alzheimer's disease. Clinical neuropathology. 2012;31(3):116.
[30]Wilcock DM, Lewis MR, Van Nostrand WE, Davis J, Previti ML, Gharkholonarehe N, et al. Progression of amyloid pathology to Alzheimer's disease pathology in an amyloid precursor protein transgenic mouse model by removal of nitric oxide synthase 2. Journal of Neuroscience. 2008;28(7):1537-45.

[31]Dawson HN, Ferreira A, Eyster MV, Ghoshal N, Binder LI, Vitek MP. Inhibition of neuronal maturation in primary hippocampal neurons from τ deficient mice. Journal of cell science. 2001;114(6):1179-87.
[32]Rudenko LK, Wallrabe H, Periasamy A, Siller KH, Svindrych Z, Seward ME, et al. Intraneuronal tau misfolding induced by extracellular amyloid-β oligomers. Journal of Alzheimer's Disease. 2019;71(4):1125-38.
[33]Combs B, Tiernan CT, Hamel C, Kanaan NM. Production of recombinant tau oligomers in vitro. Methods in cell biology. 2017;141:45-64.
[34]LoPresti P, Szuchet S, Papasozomenos SC, Zinkowski RP, Binder L. Functional implications for the microtubule-associated protein tau: localization in oligodendrocytes. Proceedings of the National Academy of Sciences. 1995;92(22):10369-73.
[35]Lesuisse C, Martin LJ. Long-term culture of mouse cortical neurons as a model for neuronal development, aging, and death. Journal of neurobiology. 2002;51(1):9-23.
[36]Nussbaum JM, Seward ME, Bloom GS. Alzheimer disease: a tale of two prions. Prion. 2013;7(1):14-9.
[37]Goode BL, Denis PE, Panda D, Radeke MJ, Miller HP, Wilson L, et al. Functional interactions between the proline-rich and repeat regions of tau enhance microtubule binding and assembly. Molecular biology of the cell. 1997;8(2):353-65.
[38]Goedert M, Klug A, Crowther RA. Tau protein, the paired helical filament and Alzheimer's disease. Journal of Alzheimer's Disease. 2006;9(s3):195-207.
[39]Jeganathan S, von Bergen M, Brutlach H, Steinhoff H-J, Mandelkow E. Global hairpin folding of tau in solution. Biochemistry. 2006;45(7):2283-93.
[40]Von Bergen M, Friedhoff P, Biernat J, Heberle J, Mandelkow E-M, Mandelkow E. Assembly of τ protein into Alzheimer paired helical filaments depends on a local sequence motif (306VQIVYK311) forming β structure. Proceedings of the National Academy of Sciences. 2000;97(10):5129-34.
[41]Von Bergen M, Barghorn S, Biernat J, Mandelkow E-M, Mandelkow E. Tau aggregation is driven by a transition from random coil to beta sheet structure. Biochimica et Biophysica Acta (BBA)-Molecular Basis of Disease. 2005;1739(2-3):158-66.
[42]Lee G, Neve RL, Kosik KS. The microtubule binding domain of tau protein. Neuron. 1989;2(6):1615-24.
[43]Eidenmüller J, Fath T, Hellwig A, Reed J, Sontag E, Brandt R. Structural and functional implications of tau hyperphosphorylation: information from phosphorylation-mimicking mutated tau proteins. Biochemistry. 2000;39(43):13166-75.
[44]Barthélemy NR, Bateman RJ, Hirtz C, Marin P, Becher F, Sato C, et al. Cerebrospinal fluid phospho-tau T217 outperforms T181 as a biomarker for the differential diagnosis of Alzheimer’s disease and PET amyloid-positive patient identification. Alzheimer's research & therapy. 2020;12(1):1-11.
[45]Swanson E, Breckenridge L, McMahon L, Som S, McConnell I, Bloom GS. Extracellular tau oligomers induce invasion of endogenous tau into the somatodendritic compartment and axonal transport dysfunction. Journal of Alzheimer's Disease. 2017;58(3):803-20.
[46]Alonso AdC, Zaidi T, Novak M, Grundke-Iqbal I, Iqbal K. Hyperphosphorylation induces self-assembly of τ into tangles of paired helical filaments/straight filaments. Proceedings of the National Academy of Sciences. 2001;98(12):6923-8.

[47]Haase C, Stieler J, Arendt T, Holzer M. Pseudophosphorylation of tau protein alters its ability for self-aggregation. Journal of neurochemistry. 2004;88(6):1509-20.
[48]Rajbanshi B, Mandell JW, Bloom GS. Localization, induction, and cellular effects of tau-phospho-threonine 217. bioRxiv. 2022.
[49]Grienberger C, Konnerth A. Imaging calcium in neurons. Neuron. 2012;73(5):862-85.
[50]Nevian T, Sakmann B. Spine Ca2+ signaling in spike-timing-dependent plasticity. Journal of Neuroscience. 2006;26(43):11001-13.
[51]Sabatini BL, Oertner TG, Svoboda K. The life cycle of Ca2+ ions in dendritic spines. Neuron. 2002;33(3):439-52.
[52]Miyamoto T, Stein L, Thomas R, Djukic B, Taneja P, Knox J, et al. Phosphorylation of tau at Y18, but not tau-fyn binding, is required for tau to modulate NMDA receptor-dependent excitotoxicity in primary neuronal culture. Molecular neurodegeneration. 2017;12(1):1-19.
[53]Khan SS, LaCroix M, Boyle G, Sherman MA, Brown JL, Amar F, et al. Bidirectional modulation of Alzheimer phenotype by alpha-synuclein in mice and primary neurons. Acta neuropathologica. 2018;136(4):589-605.
[54]Kodis EJ, Choi S, Swanson E, Ferreira G, Bloom GS. N-methyl-D-aspartate receptor–mediated calcium influx connects amyloid-β oligomers to ectopic neuronal cell cycle reentry in Alzheimer's disease. Alzheimer's & Dementia. 2018;14(10):1302-12.
[55]Babaei P. NMDA and AMPA receptors dysregulation in Alzheimer's disease. European Journal of Pharmacology. 2021;908:174310.